Journal of Inflammation Research

Dovepress
Taylor & Francis Group

Open Access Full Text Article

ORIGINAL RESEARCH

High-Altitude Hypoxic Preconditioning Attenuates Lipopolysaccharide-Induced Lung Injury and is Associated with Alveolar-Capillary Barrier Maintenance

Ruixuan Wang[1,*], Yu Zhang[2,*], Wantian Zhang[1,*], Mei Gong[1], Danyang Zhao[1], Wei Chen[1], Chunhua Chen[3], Qian Lei[1], Si Zeng[1,4]

[1]Department of Anesthesiology, Sichuan Provincial People's Hospital, School of Medicine, University of Electronic Science and Technology of China, Chengdu, Sichuan, People's Republic of China; [2]Department of Anesthesiology, Sports Hospital Affiliated to Chengdu Sports Institute, Chengdu, Sichuan, People's Republic of China; [3]Department of Anatomy and Embryology, School of Basic Medical Sciences, Peking University Health Science Center, Beijing, People's Republic of China; [4]Department of Anesthesiology, Bazhong Central Hospital, Bazhong, Sichuan, People's Republic of China

*These authors contributed equally to this work

Correspondence: Si Zeng; Qian Lei, Department of Anesthesiology, Sichuan Provincial People's Hospital, School of Medicine, University of Electronic Science and Technology of China, Chengdu, Sichuan, People's Republic of China, Email xzyxyzs@hotmail.com; leiqianggh@163.com

Introduction: High-altitude hypoxic preconditioning (HAP) is an adaptive state induced by sustained exposure to hypobaric hypoxia. In addition to improving tolerance to hypoxia itself, HAP may also modify organ responses to subsequent inflammatory stress. The alveolar-capillary barrier is essential for maintaining pulmonary structural integrity, fluid balance, and gas exchange, and its disruption is a central event in inflammatory lung injury. However, whether HAP-related pulmonary protection is associated with preservation of the alveolar-capillary barrier and coordinated changes in barrier-related cells remains unclear. This study aimed to investigate the effects of HAP on alveolar-capillary barrier preservation under lipopolysaccharide (LPS) challenge and to explore the associated cellular transcriptional characteristics.

Methods: A rat model of HAP was established by exposure to hypobaric hypoxia for 4 weeks. Rats were assigned to four groups: normoxic control (C), normoxia+LPS (CL), HAP control (H), and HAP+LPS (HL). Gross lung appearance, lung dry/wet ratio, histopathology, inflammatory and oxidative stress markers, and arterial blood gas parameters were evaluated. Single-cell RNA sequencing was performed in the CL and HL groups to assess transcriptional changes in endothelial cells, epithelial cells, and macrophages. Transmission electron microscopy and immunofluorescence staining for VE-cadherin and E-cadherin were used to evaluate barrier ultrastructure and junctional integrity.

Results: Compared with the CL group, the HL group showed reduced pulmonary edema, less exudation and congestion, milder histological damage, and better oxygenation under LPS challenge. Lactate elevation was attenuated and metabolic changes were less pronounced in the HL group. Single-cell transcriptomic analysis showed distinct transcriptional characteristics in barrier-related cells after HAP. Endothelial cells in the HL group exhibited increased expression of genes related to cell junctions and cytoskeletal organization, epithelial cells exhibited upregulated expression of genes associated with cell membrane structure, cell adhesion, and alveolar fluid clearance, accompanied by an increased proportion of AT1 cells and a decreased proportion of tuft cells. Macrophages tended to express more repair-related genes. In contrast, the CL group showed more stress-, injury-, inflammation-, and interferon-related transcriptional features. Ultrastructural examination demonstrated better preservation of endothelial and alveolar epithelial integrity in the HL group. Immunofluorescence analysis further showed stronger and more continuous VE-cadherin and E-cadherin signals in the HL group than in the CL group.

Conclusion: HAP was associated with better preservation of the alveolar-capillary barrier under LPS challenge, as reflected by reduced pulmonary edema, improved oxygenation, stronger junctional protein signals, and better preserved barrier structure. This barrier-protective effect was accompanied by coordinated transcriptional changes in endothelial cells, epithelial cells, and macrophages.

Keywords: high-altitude hypoxic preconditioning, alveolar-capillary barrier, acute lung injury, alveolar epithelial cells, environmental adaptation

https://doi.org/10.2147/JIR.S577600
Received: 6 November 2025
Accepted: 18 May 2026
Published: 13 June 2026

Graphical Abstract

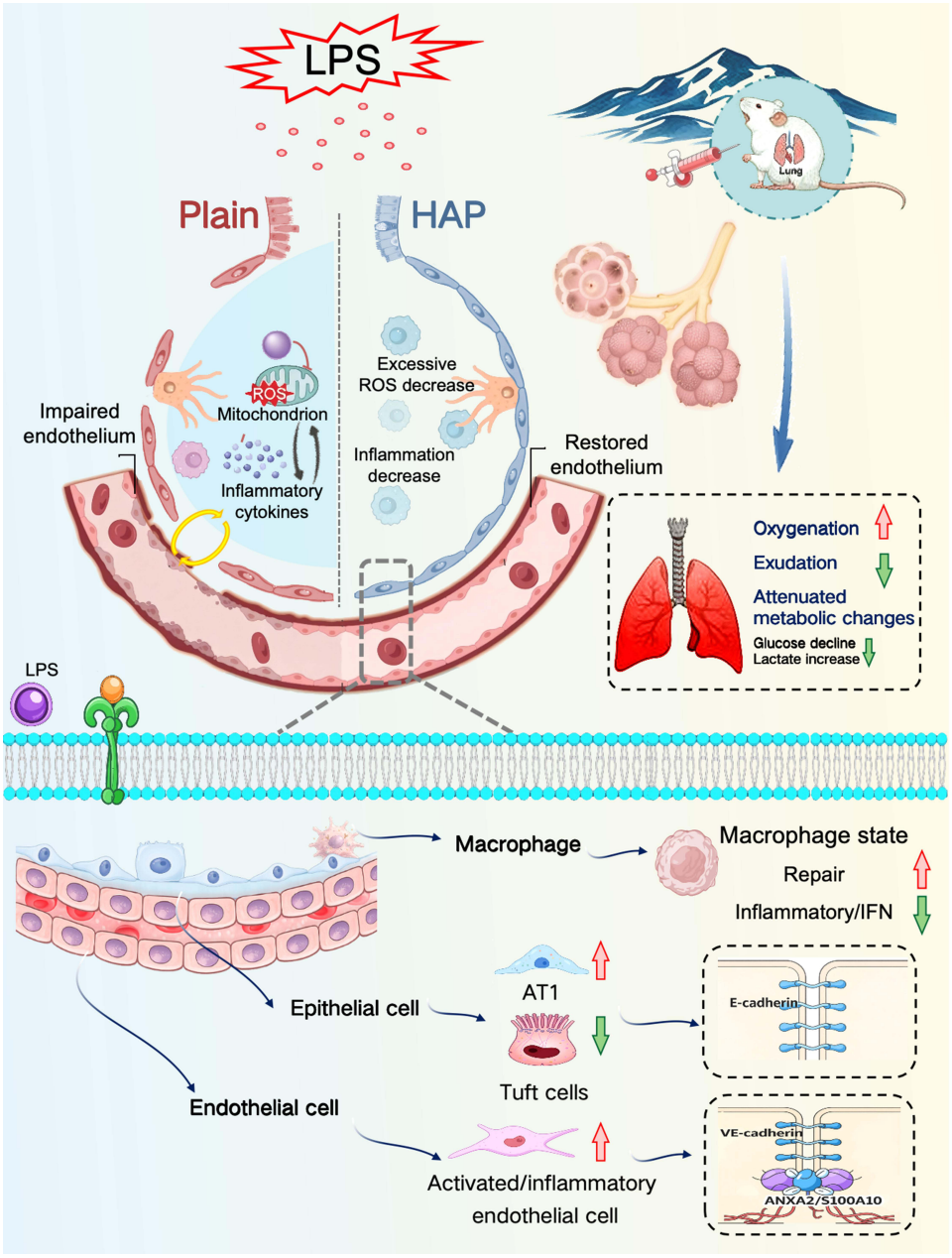

Introduction

The fundamental physiological characteristics of the high-altitude environment are decreased atmospheric pressure and reduced inspired partial pressure of oxygen,[1] which constitute an important natural environmental stressor to which the body is chronically exposed. Previous studies on high-altitude hypoxia have mainly focused on the mechanisms underlying acute hypoxic injury and high-altitude-related diseases, and it is generally believed that a hypobaric hypoxic environment may induce adverse effects such as aggravated oxidative stress, abnormal organ perfusion, and tissue dysfunction.[2–4] However, with prolonged exposure, the body can gradually establish an adaptive state, which is characterized by enhanced oxygen transport capacity,[5] altered metabolic regulatory patterns,[6] and upregulation of

antioxidant-related genes.[7] Existing studies suggest that this adaptive process is associated with activation of hypoxia-inducible factor (HIF)-related signaling pathways; HIF may promote adaptation to sustained hypoxic environments by participating in erythropoiesis, angiogenesis, energy metabolic remodeling, and regulation of redox homeostasis.[8,9] High-altitude hypoxic preconditioning (HAP) is precisely an adaptive state formed after sustained exposure to hypobaric hypoxia. Therefore, its significance may not be limited to improving tolerance to hypoxia itself, but may also extend to influencing organ responses to subsequent inflammatory or injurious stimuli.

The lung is one of the earliest organs directly exposed to a hypobaric hypoxic environment and is also an important target organ susceptible to functional imbalance under various stress conditions.[10] Acute lung injury (ALI) and its severe stage, acute respiratory distress syndrome, are common and serious complications associated with infection, sepsis, trauma, and the perioperative period.[11,12] One of the major pathological bases of these conditions is injury to the alveolar-capillary barrier, manifested by increased permeability, fluid leakage, pulmonary edema, and impaired oxygenation. The alveolar-capillary barrier provides the structural basis for maintaining pulmonary tissue stability, normal gas exchange, and fluid balance.[13,14] This barrier is mainly composed of pulmonary microvascular endothelial cells, alveolar epithelial cells, and the intervening basement membrane.[15,16] Among these, endothelial cells are involved in the regulation of vascular permeability;[17,18] epithelial cells maintain the integrity of intercellular junctions within the alveoli and participate in alveolar fluid clearance;[19,20] macrophages, in turn, are involved throughout the processes of alveolar-capillary barrier injury and repair.[21,22] Under physiological conditions, these cells regulate one another, and during the progression of lung injury they interact through cytokine release, chemotactic signal transmission, and changes in structural responses. Therefore, the effects of HAP may not be confined to a single cell type, but may simultaneously influence the response states of endothelial cells, epithelial cells, and macrophages, thereby affecting the extent of alveolar-capillary barrier injury under inflammatory stimulation.

Our previous studies showed that long-term HAP was associated with a reduced incidence of perioperative major adverse cardiovascular events and attenuated postoperative myocardial injury in patients undergoing cardiac surgery, suggesting that HAP may enhance tolerance to ischemia-reperfusion injury and thereby exert organ-protective effects.[23] To further explore its potential multi-organ protective effects, our team subsequently established a prospective propensity score-matched clinical cohort of patients undergoing hepatectomy. The results showed that, compared with the lowland population, individuals residing long-term at altitudes of ≥1500 m had a lower incidence of postoperative pulmonary complications within 7 days after surgery and milder complications, as reflected by a lower incidence of pleural effusion and a shorter length of hospital stay;[24] multivariable regression analysis further suggested that HAP is an important protective factor against perioperative pulmonary complications. In animal experiments, our team previously established a rat model of HAP combined with sepsis-induced acute lung injury. The results showed that, compared with conventional controls, HAP treatment markedly attenuated pulmonary inflammatory injury and improved oxygenation, suggesting that HAP may enhance tolerance to stress-induced lung injury.[25] These clinical observations and animal experimental findings suggest that HAP-related pulmonary protection may not be limited to changes in inflammatory responses per se, but may also be related to better preservation of the structure and function of the pulmonary tissue barrier. Although previous studies have suggested that HAP may exert protective effects against lung injury, direct evidence is still lacking as to whether it confers such protection by modulating alveolar-capillary barrier-related cells. Therefore, exploring endogenous pulmonary protection and its related cellular basis from the perspective of high-altitude hypoxic preconditioning is of scientific significance.

Based on the above background and our previous work, the present study employed an HAP rat model and established an acute lung injury model by lipopolysaccharide (LPS) induction. Using a comprehensive approach that included histopathological observation, measurement of inflammatory and oxidative stress markers, arterial blood gas analysis, single-cell transcriptomic sequencing, transmission electron microscopy, and immunofluorescence staining, this study analyzed the effects of high-altitude hypoxic preconditioning at multiple levels, including structure, function, and cellular state. Specifically, this study aimed to investigate, from the perspective of changes in barrier-related cells, the effects of high-altitude hypoxic preconditioning on acute lung injury and to provide evidence for understanding the endogenous pulmonary protective effects of HAP.

Materials and Methods

Animal Model

Experimental procedures were performed using healthy 6-week-old male Sprague–Dawley (SD) rats. The animals were purchased from the Experimental Animal Institute of Sichuan Provincial People's Hospital. All procedures involving animal use and disposal were approved by the Basic and Clinical Research Ethics Committee of Sichuan Provincial People's Hospital (Approval No. 2024–419) and were conducted in accordance with the principles of the 3Rs. Animals were housed under controlled conditions, with a temperature of 25 ± 2°C, a 12-h light/dark cycle, and free access to food and water. Male animals were used to minimize the potential effects of the estrous cycle on alveolar epithelial physiology and inflammatory responses. All statistical analyses were performed using individual animals as the unit of biological replication; unless otherwise specified, n refers to the number of animals included in a given analysis rather than the number of technical replicates.

The rats were randomly assigned to four groups: the normoxic control group (C), normoxia + LPS group (CL), high-altitude hypoxic preconditioning control group (H), and high-altitude hypoxic preconditioning + LPS group (HL). Randomization was performed using a random number table, with each rat assigned a unique number prior to grouping to ensure allocation concealment. Rats in the H and HL groups were housed in a hypobaric hypoxic chamber (ProOx-811, Shanghai Tower Sci-Tech, China) for 4 weeks, with the chamber preset to simulate an altitude of 4000 m (approximately 62.0 kPa atmospheric pressure). Rats in the C and CL groups were housed in the same animal facility during the same period. After the exposure period, rats in the CL and HL groups received intraperitoneal injection of lipopolysaccharide (LPS, 15 mg/kg; Sigma-Aldrich, L2630-100 mg) according to body weight to establish an acute lung injury model, whereas rats in the C and H groups received an equal volume of normal saline by intraperitoneal injection. Six hours after injection, the rats were anesthetized with sevoflurane, and abdominal aortic blood and inferior vena cava blood were collected. The animals were then euthanized by exsanguination under deep anesthesia, and lung tissues were harvested for subsequent analyses.

Animal Inclusion and Exclusion Criteria and Sample Size

The design, conduct, and reporting of this study followed the ARRIVE 2.0 guidelines.[26] Upon arrival, animals with evidence of infection, injury, or obvious behavioral abnormalities were excluded from the experiment. Animals were allocated to different experimental groups using a random number table.During high-altitude hypoxic exposure, animals showing severe stress responses, including marked weight loss, lethargy, or dyspnea, were excluded according to predefined criteria. No post hoc, outcome-driven exclusions were performed during the statistical analysis stage.

The sample size was determined primarily with reference to our team's previous studies using similar models and the feasibility of the present study. For conventional phenotypic analyses, including serum TNF-α and MDA measurement, lung dry/wet weight ratio, H&E staining, and arterial blood gas analysis, 6 animals were included in each group. For immunofluorescence analysis, 4 animals were included in each group. For transmission electron microscopy analysis, 3 animals were included in each group. For single-cell RNA sequencing, only the CL and HL groups were included, with 3 animals in each group.

Measurement of Inflammatory Cytokines and Oxidative Stress Markers

Approximately 5 mL of blood was collected from the inferior vena cava before euthanasia and centrifuged at 4°C and 3000×g for 15 min. After serum separation, the samples were stored at −80°C. Commercial ELISA kits were used to determine serum concentrations of tumor necrosis factor-α (TNF-α; RX2D2027606, Ruixin Bio, China) and malondialdehyde (MDA; JRX202066, Ruixin Bio, China), and all procedures were performed in accordance with the manufacturers' instructions. Briefly, standard wells, blank wells, and sample wells were set up in a 96-well plate. After the appropriate standards or samples were added to each well, HRP-labeled detection antibody was added to all wells except the blank wells, followed by incubation at 37°C for 1 h. After washing the plate 5 times, substrate working solution was added, and the plate was incubated at 37°C in the dark for approximately 15 min. The reaction was then terminated by adding stop solution, and the absorbance was measured at 450 nm. Sample concentrations were calculated based on the standard curve.

Histopathological Examination of Lung Tissue

Immediately after collection, the lungs were grossly examined for color, surface congestion, and hemorrhage, and photographs were taken for documentation. Surface fluid was gently blotted off the lung tissue with absorbent paper, and the wet weight (W) was measured. The tissue was then dried in a constant-temperature oven at 80°C for 48 h to obtain the dry weight (D). The dry/wet weight ratio (D/W) was calculated to evaluate the degree of pulmonary edema. Lung tissue for histological analysis was fixed, routinely dehydrated, cleared, paraffin-embedded, and sectioned at 4 μm, followed by hematoxylin and eosin (H&E) staining. Sections were examined under a light microscope and images were acquired. H&E results are presented as representative images.

Arterial Blood Gas Analysis

After opening the abdominal cavity as described above, arterial blood was collected from the abdominal aorta using a heparinized syringe and immediately analyzed with a blood gas analyzer (iSTAT1, Abbott, USA). The recorded parameters included pH, PO_2, PCO_2, BE, HCO^{3-}, TCO_2, SO_2, lactate, Hct, and Hb. Arterial oxygen content (CaO_2) was calculated based on Hb, SO_2, and PO_2.

Single-Cell RNA Sequencing Analysis

In the present study, the purpose of single-cell analysis was to focus on cellular differences associated with the HAP-related protective phenotype under inflammatory stimulation rather than to comprehensively characterize the high-altitude adaptation profile under basal conditions. Therefore, single-cell RNA sequencing was performed only in the CL and HL groups.

Three rats were randomly selected from each group. Approximately 0.05 cm^3 of fresh lung tissue was collected from the left upper lobe, placed in pre-cooled single-cell sample preservation solution at 4°C, and sent to Hangzhou Lianchuan Biotechnology Co., Ltd. for subsequent tissue dissociation, library preparation, and sequencing. All single-cell sequencing and related bioinformatic analyses were completed by Hangzhou Lianchuan Biotechnology Co., Ltd. on its single-cell sequencing cloud platform. For tissue dissociation, tissue pieces were incubated in digestion solution containing 0.35% collagenase IV, 2 mg/mL papain, and 120 U/mL DNase I at 37°C and 100 rpm for 20 min. The reaction was then terminated with PBS containing 10% FBS, followed by gentle trituration. The cell suspension was sequentially filtered through 70 μm and 30 μm cell strainers, centrifuged at 4°C and 300×g for 5 min, treated with red blood cell lysis buffer to remove erythrocytes, and subjected to dead cell removal using Dead Cell Removal MicroBeads. Cell viability was assessed by trypan blue staining and required to be >85%, and the cell concentration was adjusted to 700–1200 cells/μL. Libraries were constructed using the 10× Genomics Chromium Single-Cell 3′ Kit (V3) platform, with an expected capture of approximately 10,000 cells. After raw sequencing data were converted to FASTQ files, alignment and counting were performed using CellRanger, and the expression matrix was subsequently imported into Seurat (v4.1.0) for analysis. Low-quality cells were filtered according to the following criteria: number of detected genes per cell >500, mitochondrial gene proportion <25%, and doublets removed using DoubletFinder. After LogNormalize normalization, the top 2000 highly variable genes were selected for principal component analysis(PCA), and the first 20 principal components were used for clustering. For multisample integration, Harmony was used to correct batch effects, and UMAP was used for visualization. Differentially expressed genes were identified according to the following criteria: proportion of expressing cells in the target cell cluster >10%, $P \leq 0.01$, and $logFC \geq 0.26$. Gene Ontology(GO) enrichment analysis was performed based on the differentially expressed gene sets, and pseudotime analysis was conducted using Monocle 2.4.

Transmission Electron Microscopy

Three animals from each group were used for transmission electron microscopy. Immediately after collection, lung tissue was prefixed in 3% glutaraldehyde and then post-fixed in 1% osmium tetroxide for 1–2 h. After graded acetone dehydration, the tissue was embedded in Epon-812 resin. Ultrathin sections (60–90 nm) were cut, stained with uranyl acetate and lead citrate, and examined for pulmonary ultrastructure using a transmission electron microscope (JEM-1400FLASH, JEOL, Japan). TEM results are presented as representative images.

Immunofluorescence Staining

Four animals from each group were used for immunofluorescence analysis. After deparaffinization and rehydration, paraffin sections were subjected to heat-induced antigen retrieval in citrate buffer (pH 6.0). Endogenous peroxidase activity was blocked with 3% H2O2 for 20 min at room temperature, and after PBS washing, sections were blocked with 10% goat serum for 30 min. The sections were first incubated with primary antibody against VE-cadherin (ab33168, Abcam), followed by incubation with HRP-labeled secondary antibody (ab205718, Abcam), and signal amplification was performed using Cy3-tyramide. The sections were then incubated with primary antibody against E-cadherin (ab231303, Abcam) and the corresponding HRP-labeled secondary antibody (ab6789, Abcam) using the same procedure, and visualized with a 488 fluorescent dye. Finally, nuclei were counterstained with DAPI and the sections were mounted. After acquisition of fluorescence images, semiquantitative analysis was performed using ImageJ software. Multiple high-power fields were randomly selected for each animal, the mean fluorescence intensity was calculated for each field and then averaged to obtain the final measurement for that animal, and intergroup comparisons were performed using the individual animal as the statistical unit.

Statistical Analysis and Blinding

Statistical analysis was performed using SPSS 27.0, and graphs were generated using GraphPad Prism 10.3.1. Continuous data were first tested for normality and homogeneity of variance. Measurement data conforming to a normal distribution and homogeneity of variance are presented as mean±standard deviation (mean±SD). Comparisons among multiple groups were performed using one-way analysis of variance (one-way ANOVA), and post hoc pairwise comparisons were conducted using the Tukey's test. A $P<0.05$ was considered statistically significant. Statistical significance in the figures is indicated as follows: *$P<0.05$, **$P<0.01$, ***$P<0.001$, ****$P<0.0001$.

With regard to blinding, investigators involved in ELISA measurement, immunofluorescence image acquisition, and semiquantitative analysis were unaware of group allocation during the measurement and analysis stages; blinding was not implemented in the other experimental procedures.

Results

HAP Attenuates Inflammation and Morphological Lung Injury in Rats After LPS Stimulation

No obvious abnormalities in general condition were observed in the C group. Compared with the C group, rats in the H group showed no obvious abnormalities in general condition, except for slightly darker coloration of the nose and oral region. During the pre-experimental feeding period, no deaths or abnormalities in general condition occurred in either the C group or the H group. After LPS stimulation, rats in the CL group exhibited lethargy, sluggish responses, obvious piloerection, shallow and rapid breathing, marked anorexia, and loose or bloody stools. In contrast, the general condition of the HL group was improved compared with that of the CL group. Although piloerection and shallow tachypnea were still observed, anorexia was less severe, and the stools were basically formed and close to normal.

To investigate the effects of HAP on systemic inflammation and oxidative stress in rats after LPS stimulation, we measured serum levels of MDA and TNF-α in each group by ELISA (Figure 1A and B). The results showed that, compared with the C group, no significant changes were observed in any of these indicators in the H group ($P>0.05$). After LPS stimulation, serum MDA and TNF-α levels in the CL group were significantly increased compared with those in the C group (both $P<0.0001$). Further comparison showed that the TNF-α level in the HL group was lower than that in the CL group ($P<0.01$), whereas there was no statistically significant difference in MDA level between the CL group and the HL group ($P>0.05$). Notably, TNF-α and MDA levels in the HL group did not differ significantly from those in the H group.

To preliminarily assess lung injury, gross observation and measurement of the lung dry/wet weight ratio were performed. As shown in Figure 1C, the lungs in the C group were pale pink, without obvious congestion or edema; the lungs in the H group were darker in color and showed mild congestion. After LPS stimulation, pulmonary congestion was markedly aggravated in the CL group, and multiple scattered hemorrhagic spots were visible on the lung surface,

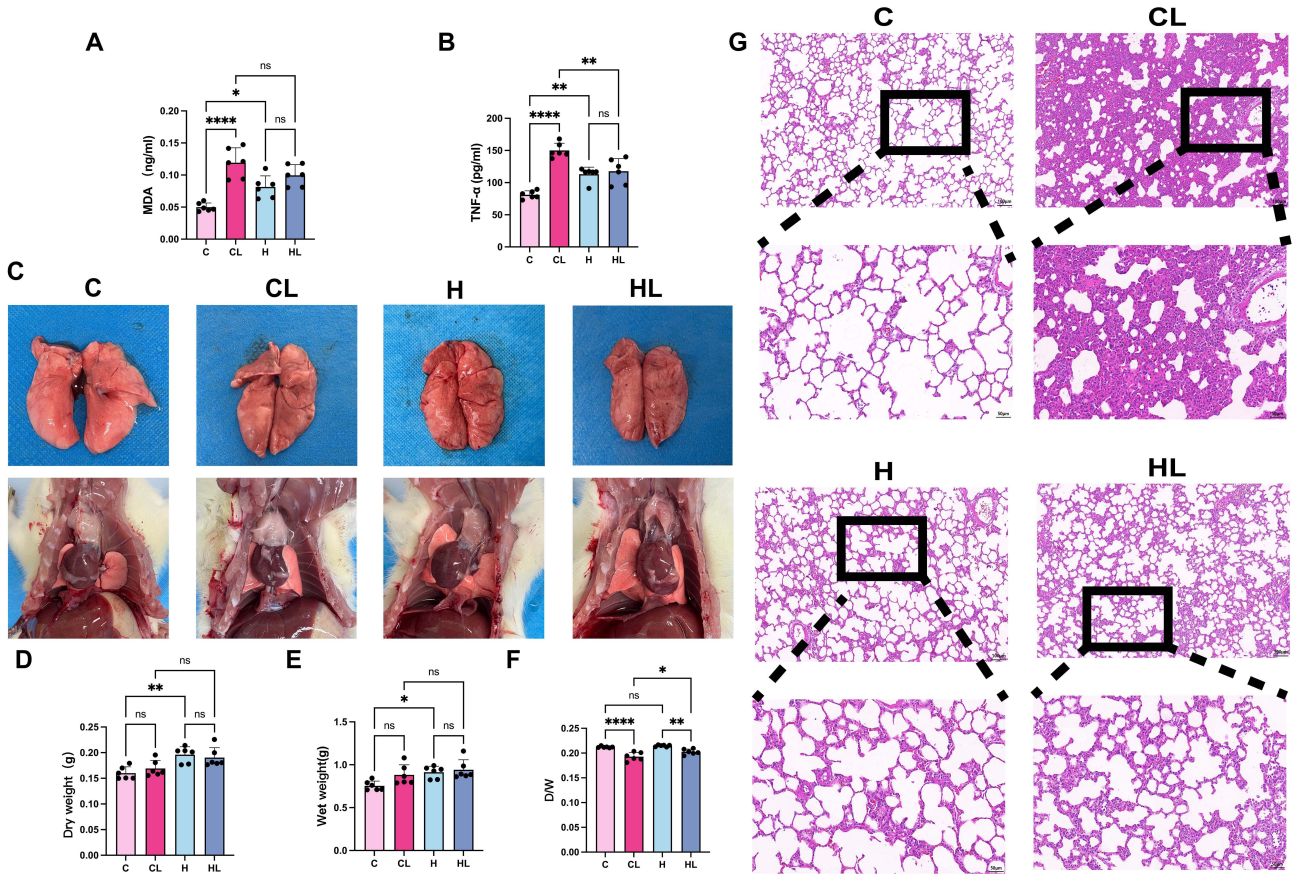

Figure 1 HAP attenuates LPS-induced systemic inflammation and acute lung injury (n = 6). (**A**) Serum MDA levels. (**B**) Serum TNF-α levels. (**C**) Representative images of the lungs and thoracic cavity in each group. (**D**) Dry lung weight. (**E**) Wet lung weight. (**F**) Dry/wet lung weight ratio. (**G**) Representative H&E-stained images of lung tissue.Scale bars: 100μm; 50μm.C group, normoxic control group; CL group, normoxia+LPS group; H group, HAP control group; HL group, HAP+LPS group.ns, not significant; *P<0.05, **P<0.01, ***P<0.001, ****P<0.0001.

whereas only a few scattered congestive spots were observed in the HL group. Further measurement of the lung dry/wet weight ratio showed that, compared with their respective control groups, both the CL group and the HL group exhibited decreased dry/wet ratios, with a more pronounced decrease in the CL group. Compared with the HL group, the dry/wet ratio was significantly lower in the CL group (P<0.05) (Figure 1D–F).

H&E staining further showed (Figure 1G) that lung architecture in the C group was basically normal, with regular alveolar morphology, clear and patent alveolar spaces, thin alveolar septa, and no obvious interstitial edema. In the H group, the overall lung structure remained relatively intact, the alveolar spaces were basically clear, and the alveolar septa were mildly thickened compared with those in the C group, without obvious exudation or congestion. After LPS stimulation, the CL group showed the most prominent histopathological changes, characterized by narrowed alveolar spaces, focal alveolar collapse, disorganized alveolar architecture, marked interstitial edema, and inflammatory cell infiltration in both the alveolar spaces and interstitium. In contrast, although a certain degree of injury was still present in the HL group, it was markedly attenuated compared with that in the CL group, as evidenced by relatively preserved alveolar morphology, only small amounts of proteinaceous exudate in some alveolar spaces, and less severe alveolar septal thickening, interstitial edema, and inflammatory cell infiltration than in the CL group.

Taken together, compared with the CL group, the HL group exhibited a milder systemic inflammatory response, reduced pulmonary exudation and congestion, less severe pulmonary edema, and markedly alleviated histological injury, suggesting that HAP attenuates inflammation and morphological lung injury in rat lungs after LPS stimulation.

https://doi.org/10.2147/JIR.S577600

HAP Improves Oxygenation-Related Parameters and Attenuates Lactate Elevation After LPS Stimulation

In conjunction with the above morphological changes and changes in lung water content, we further performed arterial blood gas analysis to evaluate oxygenation, acid-base status, and metabolic parameters in each group of rats.

The results showed that there were no statistically significant differences in Hb, Hct, or CaO2 between the two lowland groups, whereas both the H group and the HL group had higher levels than the lowland groups. Specifically, Hb and Hct were both markedly increased in the H group and HL group, with correspondingly higher CaO_2 values (all $P<0.0001$)(Figure 2A–C). After LPS stimulation, SO_2 and PO_2 in the CL group were both significantly lower than those in the HL group (both $P<0.05$), and CaO_2 was also significantly lower than that in the HL group ($P<0.0001$)(Figure 2C–E). Although there were some differences in PCO_2 among the groups, the mean values in all groups remained within the normal range (Figure 2F).

Analysis of acid-base- and metabolism-related parameters showed that there were overall differences in pH, BE, HCO^{3-}, and TCO_2 among the groups (Figure 2G–J). Compared with the lowland groups, the high-altitude groups showed more pronounced changes in acid-base parameters. Among them, the HL group had the lowest pH, a more negative BE, and the lowest HCO^{3-} and TCO_2 levels. The H group also showed decreased BE accompanied by reduced HCO_{3-} and TCO_2, although to a lesser extent than the HL group. Lactate levels also differed significantly among the groups, with the CL group showing significantly higher lactate levels than the HL group ($P<0.05$) (Figure 2K). Blood glucose was significantly lower in the CL group than in the C group, whereas no significant differences were observed in the other pairwise comparisons (Figure 2L).

Taken together, HAP-treated rats exhibited higher levels of Hb, Hct, and CaO_2. Under LPS stimulation, the HL group showed higher SO_2, PO_2, and CaO_2 than the CL group, along with smaller increases in lactate and smaller decreases in blood glucose, suggesting that HAP improves oxygenation-related parameters after acute lung injury and attenuates metabolic disturbances.

Single-Cell Transcriptomic Analysis Showed That HAP Affects the Transcriptional Characteristics of Alveolar-Capillary Barrier-Related Cells

The above results showed that, after HAP treatment, LPS-induced changes in gross lung appearance, inflammation- and oxidative stress-related indicators, histological injury, and oxygenation-related parameters were all attenuated compared with those in the CL group. To further examine, at the cellular level, the effects of HAP on the transcriptional characteristics of key cell populations in lung tissue, single-cell RNA sequencing was performed on lung tissues from rats in the CL and HL groups. Considering that the alveolar-capillary barrier is mainly composed of alveolar epithelial cells and pulmonary microvascular endothelial cells, and that macrophages are important inflammatory response cells in lung tissue whose changes in abundance and functional state are closely related to pulmonary barrier homeostasis, subsequent analyses focused on further subclustering and transcriptional characterization of endothelial cells, epithelial cells, and macrophages.

Major Cell Clustering Results

Single-cell sequencing data were processed according to the workflow shown in Figure 3 A. Strict quality control was performed prior to cell annotation, including filtration of cells with low gene numbers, excessive UMI counts, and high mitochondrial gene ratios, as well as removal of doublets using standard bioinformatic pipelines (Figure 3B and C). After QC filtering, lung cells were annotated based on canonical marker genes, and a total of eight major cell populations were identified: epithelial cells (Epcam, Krt8), endothelial cells (Pecam1, Cdh5), stromal cells (Tcf21, Dcn), B cells (Cd74, Ms4a1), T cells (Trbc1, Cd3g), NK cells (Nkg7, Gzma), neutrophils (S100a9, S100a8), and macrophages (Aif1, Cd68). These cell populations formed relatively distinct clusters on the UMAP plot with clear separation among different cell types (Figure 3D and E). DotPlot results confirmed that each cell population specifically expressed its characteristic marker genes, which was highly consistent with the cell annotation (Figure 3F). Comparison of cellular composition

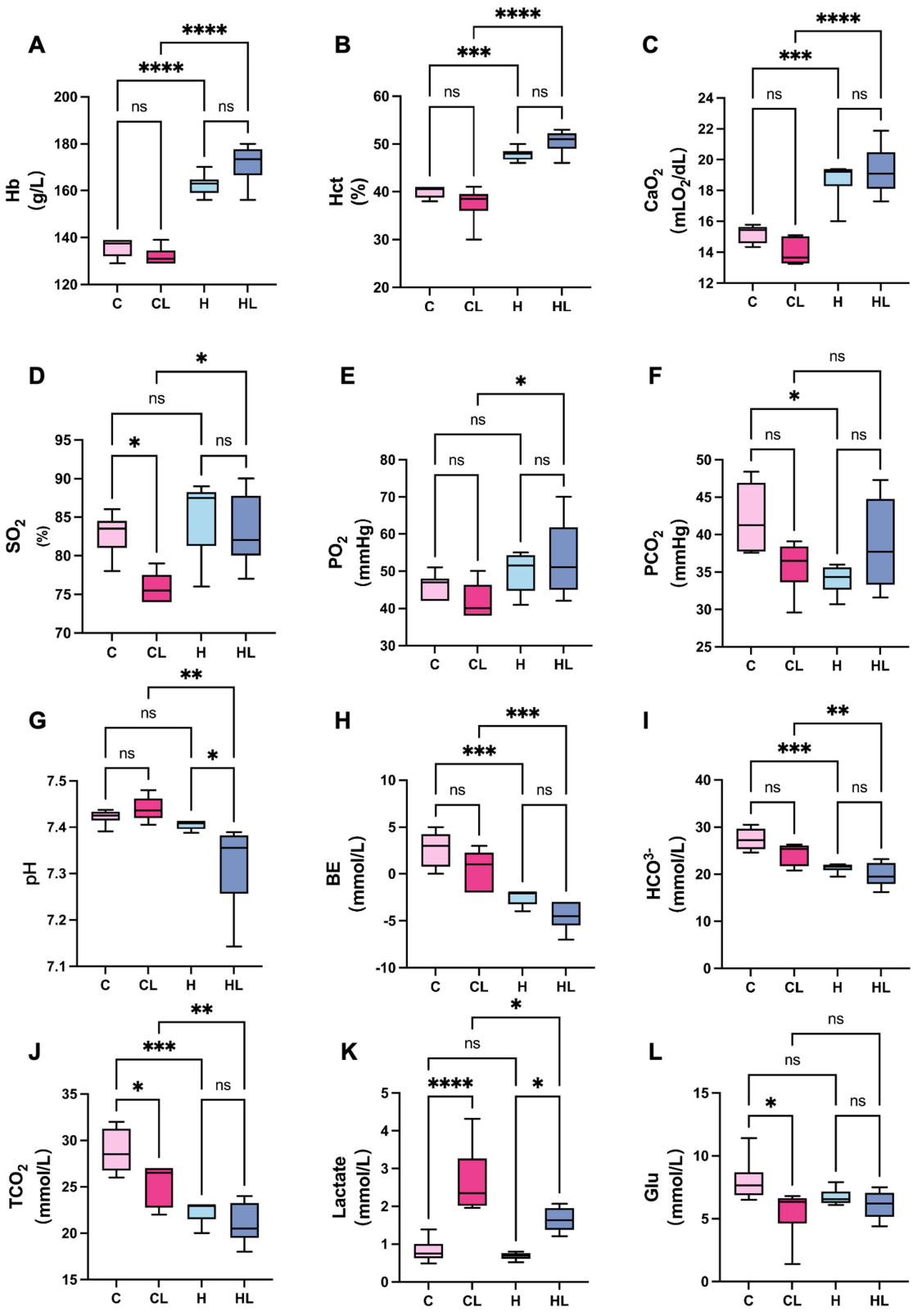

Figure 2 HAP improves oxygenation-related parameters and attenuates lactate elevation after LPS stimulation (n = 6). (**A**) Hb. (**B**) Hct. (**C**) CaO_2. (**D**) SO_2. (**E**) PO_2. (**F**) PCO_2. (**G**) pH. (**H**) BE. (**I**) HCO^{3-}. (**J**) TCO_2. (**K**) Lactate. (**L**) Blood glucose.C group, normoxic control group; CL group, normoxia+LPS group; H group, HAP control group; HL group, HAP+LPS group.ns, not significant; *P<0.05, **P<0.01, ***P<0.001, ****P<0.0001.

https://doi.org/10.2147/JIR.S577600

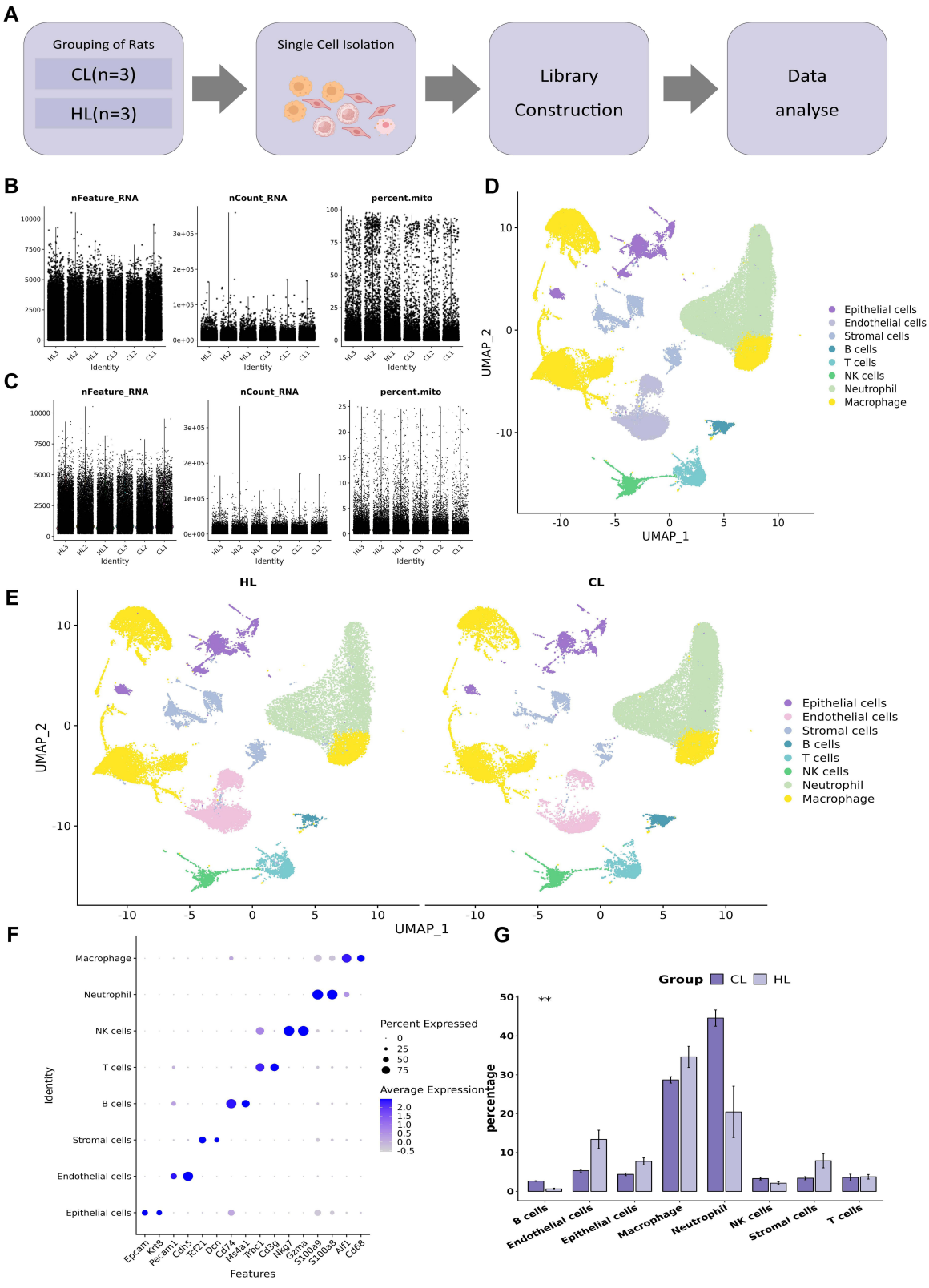

Figure 3 Single-cell transcriptomic landscape of lung tissue in rats after LPS stimulation as influenced by HAP (n=3). (**A**) Schematic diagram of the experimental design and sample-processing workflow. (**B**) The distribution of basic information of each sample cell before cell filtration. (**C**)The distribution of basic information of each sample cell after cell filtration. (**D**)UMAP plot showing clustering of all cells.(**E**)UMAP plots of the CL and HL groups. (**F**) DotPlot of canonical marker genes for each cell population. (**G**) Statistical bar plot showing differences in the proportions of each cell type between the CL and HL groups.**$P<0.01$.

https://doi.org/10.2147/JIR.S577600

between the CL and HL groups revealed that both groups contained all major cell lineages (Figure 3G), although their relative proportions differed to some extent, providing a foundation for further analysis of barrier-related cells.

HAP Alters the Transcriptional Characteristics of Pulmonary Endothelial Cells

To investigate transcriptional changes in pulmonary endothelial cells under LPS stimulation after HAP, we performed reclustering analysis of endothelial cells. Based on canonical marker genes, endothelial cells were divided into five subclusters: general capillary endothelial cells [gCap (Gpihbp1, Plvap)], aerocyte/alveolar capillary endothelial cells [aCap (Car4, Prx)], venous endothelial cells [VenEC (Ackr1, Procr)], lymphatic endothelial cells [LEC (Ccl21a, Prox1)], and one endothelial cell cluster that could not be readily assigned to the conventional subclusters described above. This cluster highly expressed Cx3cl1 and Fxyd5, accompanied by increased expression of genes such as Il6 and Ccl7, and was therefore designated, according to its initial transcriptional characteristics, as activated endothelial cells (aiEC) (Figure 4A, B, and D). In addition to expressing some inflammation-related genes, this subcluster also expressed repair-related genes such as Anxa1 and Mgp.

Comparison of cell numbers and proportions among the subclusters showed that the proportion of aiEC was higher in the HL group than in the CL group ($P<0.01$) (Figure 4C). To further examine transcriptional differences in endothelial cells between the two groups, differential expression analysis and GO enrichment analysis were performed. The results showed that upregulated genes in the CL group were mainly enriched in pathways related to response to unfolded protein, response to endoplasmic reticulum stress, and negative regulation of apoptotic process (Figure 4E), whereas upregulated genes in the HL group were mainly enriched in pathways related to extracellular exosome, focal adhesion, and actin binding (Figure 4F). Differential gene expression analysis further showed that the CL group mainly upregulated stress-related genes such as Ddit3, Xbp1, Hsp90b1, and Hspb1 (Figure 4G), whereas the HL group mainly upregulated genes related to the cytoskeleton and adhesion, including Flnb, Actr3, Vcl, and Tes (Figure 4H).

In addition, pseudotime analysis was performed on gCap, aCap, and aiEC to observe endothelial cell state transitions after LPS stimulation. The results showed that, when gCap was used as the initial state, the cell trajectory bifurcated into two major branches leading to aCap and aiEC, respectively. At the terminal end of the aiEC branch, more cells from the HL group were aggregated than from the CL group (Figure 4I and J). Pseudotime-associated gene analysis showed that S100a10 and Anxa2 expression gradually increased along the trajectory and reached peak levels at the aiEC-enriched end (Figure 4K). Combined with the group distribution pattern, the HL group was relatively enriched in the aiEC branch and was accompanied by upregulation of S100a10 and Anxa2.

Taken together, compared with the CL group, the HL group showed a higher proportion of aiEC in pulmonary endothelial cells, accompanied by increased expression of genes related to cell junctions and the cytoskeleton, whereas the CL group showed a greater tendency toward upregulation of stress-related genes. These findings reflect differences in endothelial cell states between the two groups, although the functional significance of these differences still requires further verification in subsequent experiments.

HAP Alters the Transcriptional Characteristics of Pulmonary Epithelial Cells

To investigate transcriptional changes in pulmonary epithelial cells under LPS stimulation after HAP, we performed reclustering analysis of epithelial cells and, based on canonical marker genes, classified them into five subclusters: alveolar type I epithelial cells [AT1 (Hopx, Ager)], alveolar type II epithelial cells [AT2 (Sftpc, Napsa)], secretory cells [Club cells (Scgb1a1, Scgb3a2)], ciliated cells [Ciliated cells (Foxj1, Rsph1)], and tuft cells [Tuft cells (Trpm5, Dclk1)] (Figure 5A and B).

Comparison of cell numbers and proportions among the subclusters showed that the proportion of AT1 cells was higher in the HL group than in the CL group, whereas the proportion of Tuft cells was higher in the CL group than in the HL group. There was no statistically significant difference in the number or proportion of AT2 cells between the two groups (Figure 5C). To further compare transcriptional differences in epithelial cells between the two groups, we performed differential expression analysis and GO enrichment analysis. The results showed that upregulated genes in the CL group were mainly enriched in pathways related to response to unfolded protein, unfolded protein binding, and misfolded protein binding (Figure 5D), whereas upregulated genes in the HL group were mainly enriched in pathways related to the cell membrane and cell adhesion

 https://doi.org/10.2147/JIR.S577600

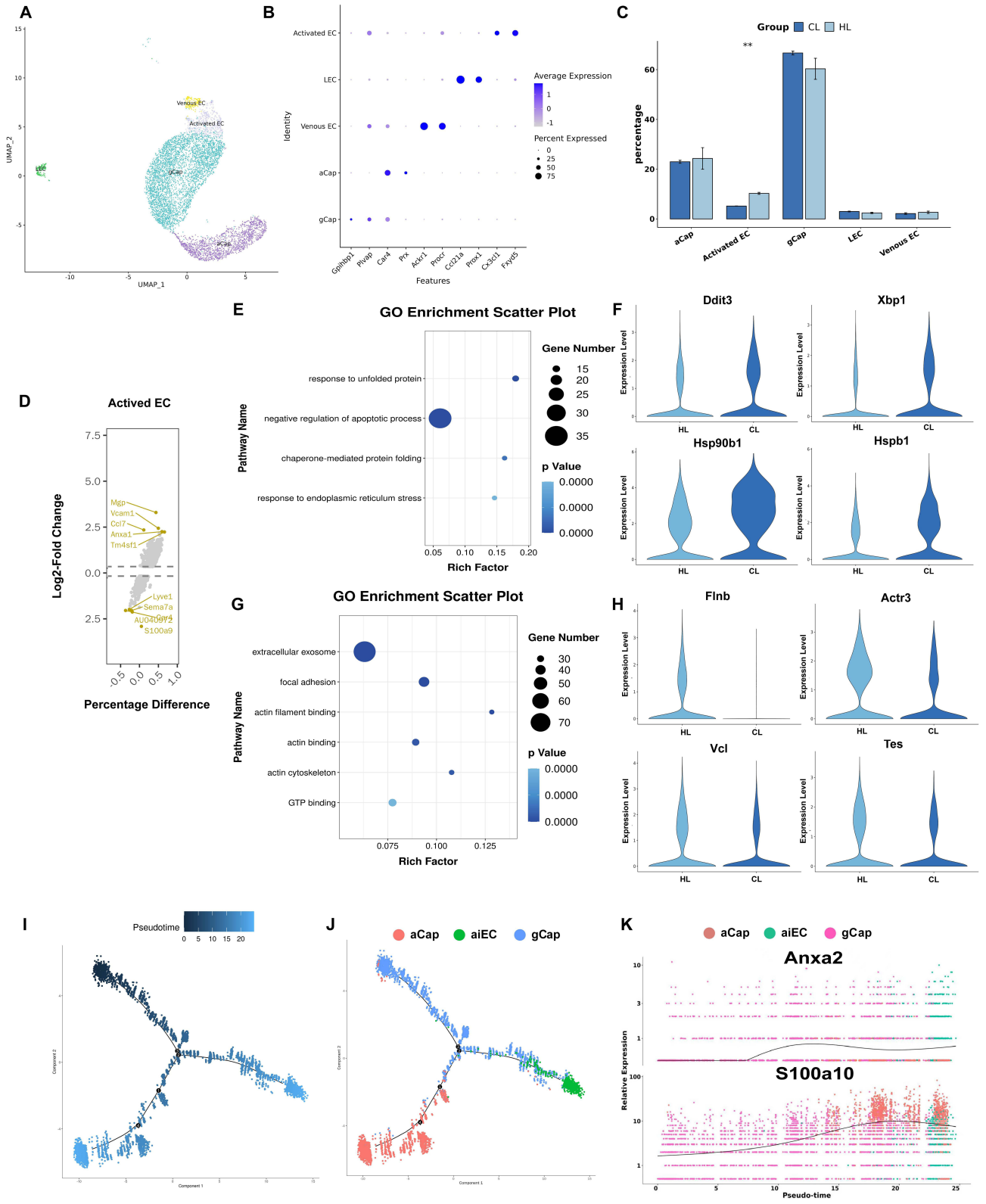

Figure 4 HAP alters the transcriptional profile of pulmonary endothelial cells (n=3). (**A**) UMAP plot of reclustered endothelial cells. (**B**) DotPlot of canonical marker genes for each endothelial cell subcluster. (**C**) Statistical bar plot showing differences in the proportions of endothelial cell subclusters between the two groups. (**D**) Volcano plot of highly expressed genes in the activated endothelial cell subcluster. (**E**) GO enrichment analysis of upregulated genes in the CL group. (**F**) GO enrichment analysis of upregulated genes in the HL group. (**G**) Violin plots of upregulated genes in the CL group. (**H**) Violin plots of upregulated genes in the HL group.(**I**) Pseudotime trajectory of pulmonary endothelial cells.(**J**) Pseudotime trajectory of pulmonary endothelial cell subclusters. (**K**) Scatter plot showing the expression levels of pulmonary endothelial cell genes along pseudotime.**P<0.01.

https://doi.org/10.2147/JIR.S577600

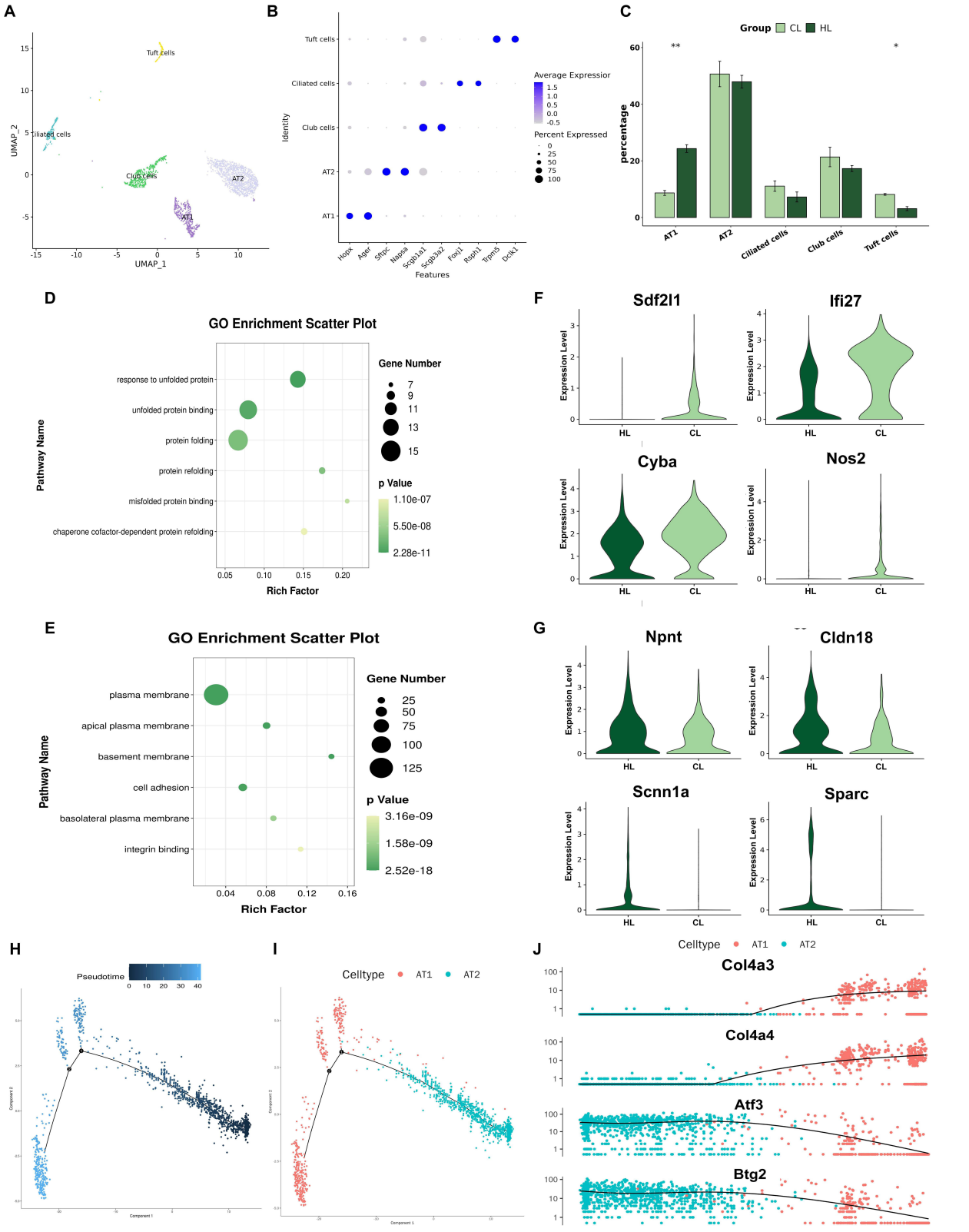

Figure 5 HAP alters the transcriptional profile of pulmonary epithelial cells in rats (n=3). (**A**) UMAP plot of reclustered epithelial cells. (**B**) DotPlot of canonical marker genes for each epithelial cell subcluster. (**C**) Statistical bar plot showing differences in the proportions of epithelial cell subclusters between the two groups. (**D**) GO enrichment analysis of upregulated genes in the CL group. (**E**) GO enrichment analysis of upregulated genes in the HL group. (**F**) Violin plots of upregulated genes in the CL group. (**G**) Violin plots of upregulated genes in the HL group. (**H**) Pseudotime trajectory of AT1 and AT2 epithelial cells in lung tissue. (**I**) Pseudotime trajectory of epithelial cell subclusters in lung tissue. (**J**) Scatter plot showing the expression levels of pulmonary epithelial cell genes along pseudotime.**P<0.01.

https://doi.org/10.2147/JIR.S577600

(Figure 5E). Differential gene expression analysis showed that genes upregulated in the CL group included Sdf2l1, Ifi27, Cyba, and Nos2 (Figure 5F), whereas genes upregulated in the HL group included Npnt, Cldn18, Scnn1a, and Sparc (Figure 5G).

In addition, pseudotime analysis was performed on AT1 and AT2 cells. The results showed differences in the distribution of cells from the two groups along the differentiation trajectory: cells from the CL group were more concentrated at the beginning of the trajectory, whereas cells from the HL group were distributed not only at the beginning but also across multiple stages of the trajectory (Figure 5H and I). Further analysis of pseudotime-associated genes showed that, during the transition from AT2 to AT1 cells, the expression of Atf3 and Btg2 gradually decreased with pseudotime, whereas the expression of Col4a3 and Col4a4 gradually increased (Figure 5J).

Taken together, compared with the CL group, the HL group showed a higher proportion of AT1 cells and a lower proportion of Tuft cells in pulmonary epithelial cells, accompanied by increased expression of genes related to membrane structure, cell adhesion, and fluid clearance, whereas the CL group showed a greater tendency toward upregulation of genes related to injury and inflammation.

HAP Alters the Transcriptional Characteristics of Pulmonary Macrophages

To investigate transcriptional changes in pulmonary macrophages under LPS stimulation after HAP, we performed reclustering analysis of macrophages and, based on canonical marker genes and transcriptional characteristics, classified them into five subclusters: mature tissue-resident alveolar macrophages [mTR-AMs (Fabp4, Pparg)], interferon-stimulated macrophages [ISMs (Ifit1, Rsad2)], inflammatory macrophages [IMs (Il1b, Nos2)], proliferating macrophages [PMs (Mki67, Top2a)], and pro-fibrotic-like macrophages [PFMs (Apoe, Trem2)] (Figure 6A and B).

Comparison of cell numbers and proportions among the subclusters showed that there was no statistically significant difference in the overall composition between the two groups, although some differences in cell composition were still observed: the proportion of inflammation-related subclusters was higher in the CL group, whereas the proportion of mature tissue-resident alveolar macrophages was higher in the HL group (Figure 6C).

To further compare transcriptional differences in macrophages between the two groups, we performed differential expression analysis and GO enrichment analysis. The results showed that upregulated genes in the CL group were mainly enriched in pathways related to inflammatory response, neutrophil chemotaxis, and positive regulation of neutrophil chemotaxis (Figure 6D), whereas upregulated genes in the HL group were mainly enriched in pathways related to the extracellular space, extracellular region, and regulation of cell proliferation (Figure 6E). Differential gene expression analysis showed that genes upregulated in the CL group included S100a9, Ptgs2, Aim2, and Ltb4r1 (Figure 6F), whereas genes upregulated in the HL group included Arg1, Anxa1, Thbd, and Timp1 (Figure 6G).

In addition, pseudotime analysis showed that macrophages from the two groups differed in their trajectory distribution. Overall, more cells from the HL group were located at the beginning of the trajectory, where mature tissue-resident alveolar macrophages predominated. Inflammatory macrophages were located at one terminal end of the trajectory, but the proportion of cells at this terminal state did not differ markedly between the two groups. At the terminal end of the interferon-stimulation-related branch, the proportion of cells from the CL group was higher than that from the HL group (Figure 6H and I). Further analysis of pseudotime-associated genes showed that Niban1 and Rgl1 were highly expressed at the beginning of the trajectory, then gradually decreased along the pro-inflammatory branch, and declined to low levels in the interferon-stimulation-related branch (Figure 6J).

Taken together, pulmonary macrophages in the HL group were overall closer to a resident-associated state, whereas those in the CL group showed greater enhancement of inflammation- and interferon-related transcriptional characteristics.

HAP Attenuates Injury to Junctional Structures of the Pulmonary Vascular and Alveolar Barriers

To observe ultrastructural changes in barrier-related cells in lung tissue after HAP, we performed transmission electron microscopy of lung tissue, focusing mainly on AT2 cells, vascular endothelial cells, and inflammatory cell infiltration within the alveolar spaces. The results showed that, in the C group, AT2 cells exhibited normal morphology, with round to oval nuclei and continuous nuclear membranes; mitochondria in the cytoplasm were morphologically intact, with

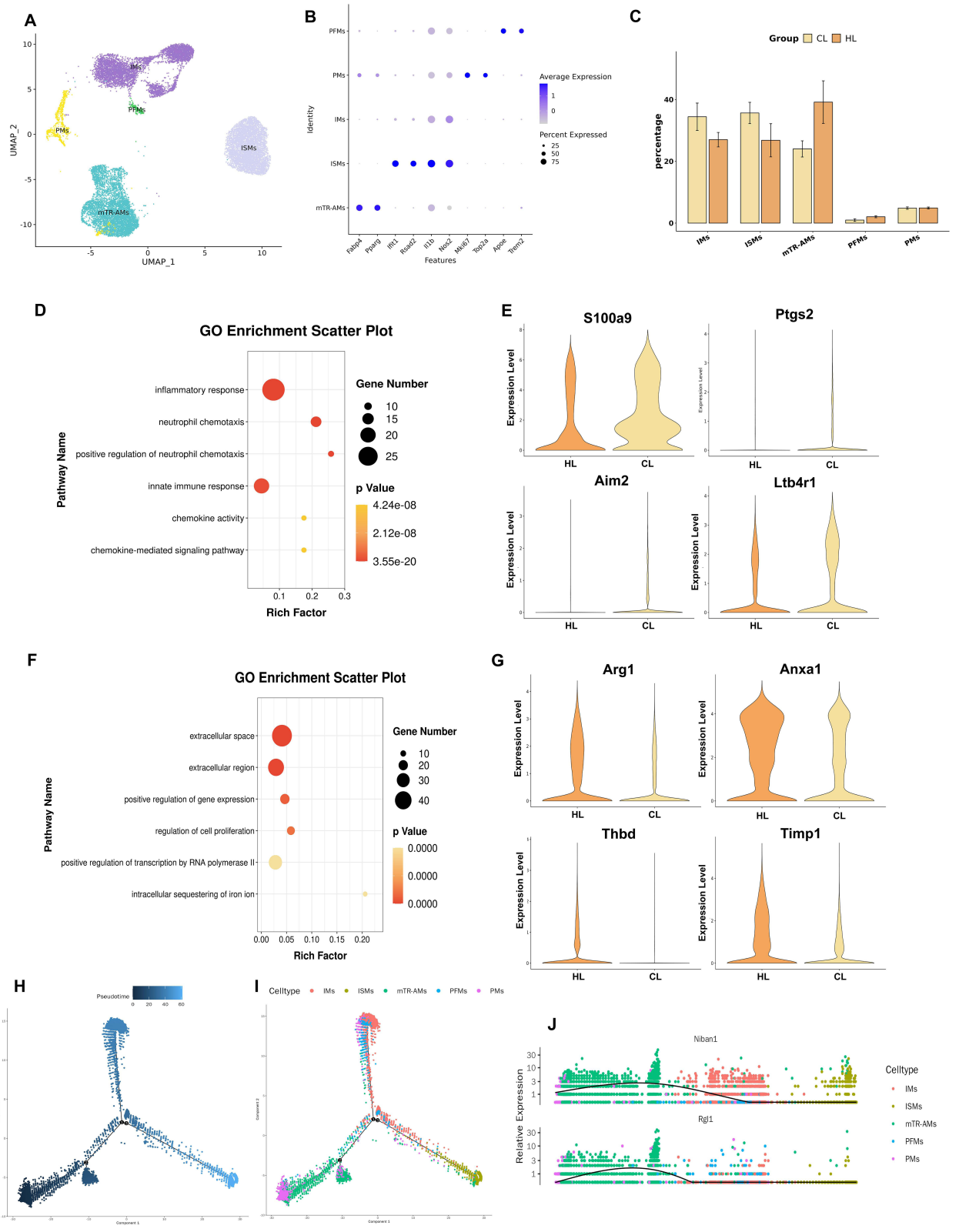

Figure 6 HAP alters the transcriptional profile of pulmonary macrophages in rats with acute lung injury (n=3). (**A**) UMAP plot of reclustered macrophages. (**B**) DotPlot of canonical marker genes for each macrophage subcluster. (**C**) Statistical bar plot showing differences in the proportions of macrophage subclusters between the two groups. (**D**) GO enrichment analysis of upregulated genes in the CL group. (**E**) GO enrichment analysis of upregulated genes in the HL group. (**F**) Violin plots of upregulated genes in the CL group. (**G**) Violin plots of upregulated genes in the HL group. (**H**) Pseudotime trajectory of macrophages in lung tissue. (**I**) Pseudotime trajectory of macrophage subclusters in lung tissue. (**J**) Scatter plot showing the expression levels of pulmonary macrophage genes along pseudotime.

https://doi.org/10.2147/JIR.S577600

clearly visible cristae, and the rough endoplasmic reticulum remained structurally intact. Vascular endothelial cells also showed normal morphology, with no obvious inflammatory cell infiltration in the alveolar spaces, and the alveolar-capillary barrier remained intact. In the H group, the overall structure of AT2 cells was likewise relatively intact, with clear and densely arranged mitochondrial cristae, and only mild vacuolar change in the rough endoplasmic reticulum; vascular endothelial cells were basically normal in morphology, and the alveolar-capillary barrier was overall preserved (Figure 7A).

After LPS treatment, ultrastructural changes in AT2 cells were most prominent in the CL group, as manifested by irregular nuclear morphology, partial disruption of the nuclear membrane, and widening of the perinuclear space. Numerous vacuolated mitochondria were observed in the cytoplasm, with disrupted or absent cristae, and the rough endoplasmic reticulum was markedly dilated. Structural abnormalities were also observed in vascular endothelial cells, including discontinuity of the nuclear membrane. Neutrophil infiltration in the alveolar spaces was increased, the alveolar-capillary barrier was markedly compressed, and the gas exchange space was reduced. In contrast, only mild ultrastructural abnormalities were observed in AT2 cells in the HL group. Nuclear morphology was slightly irregular, but the nuclear membrane remained relatively intact. Some mitochondria showed mild swelling, most mitochondrial cristae were preserved with only occasional disruption, and the rough endoplasmic reticulum was only mildly dilated. The overall structure of vascular endothelial cells was relatively preserved, and junctional structures remained present. Although neutrophil infiltration was still observed in the alveolar spaces, compression of the alveolar-capillary barrier was less severe, and some gas exchange space was still preserved (Figure 7A).

To further examine changes in adhesion junction-related proteins in the pulmonary vascular endothelium and alveolar epithelial barrier, immunofluorescence staining and semiquantitative analysis of VE-cadherin and E-cadherin were performed. The results showed that, under control conditions, VE-cadherin in the C group was distributed mainly as a continuous linear signal along intercellular junctions of pulmonary vascular endothelial cells, whereas E-cadherin was distributed mainly along the membranes of alveolar epithelial cells, showing overall relatively continuous membranous staining. In the H group, the fluorescence signals of both junctional proteins were overall stronger than those in the C group, and their distribution along cell-cell junctions remained relatively continuous (Figure 7B).

After LPS treatment, both the expression and distribution of these two adhesion junction proteins changed markedly in the CL group. The VE-cadherin fluorescence signal was evidently reduced, with focal loss of staining or disruption of continuity in some areas. The E-cadherin fluorescence signal was also weaker than that in the control group and showed a patchy distribution, accompanied by morphological changes including disorganized alveolar architecture and indistinct boundaries. Compared with the CL group, although the fluorescence signals of VE-cadherin and E-cadherin in the HL group were still reduced to some extent relative to those in the C and H groups, the overall signals were better preserved, and both proteins still showed relatively continuous distribution along cell-cell junctions. The integrity of alveolar- and vascular-related structures was also relatively better preserved (Figure 7B).

Further semiquantitative analysis of relative fluorescence intensity showed that VE-cadherin expression was strongest in the H group and was significantly higher than that in the C group and HL group (both $P<0.0001$); VE-cadherin expression in the HL group was higher than that in the CL group ($P<0.01$) (Figure 7C). Semiquantitative analysis of E-cadherin showed that expression in the C group was higher than that in the CL group ($P<0.01$), expression in the H group was higher than that in the C group ($P<0.01$), and expression in the HL group was higher than that in the CL group ($P<0.0001$) (Figure 7D).

Taken together, compared with the CL group, the HL group showed stronger fluorescence signals and better continuity of VE-cadherin and E-cadherin, suggesting that HAP attenuates injury to junctional structures of the pulmonary vascular and alveolar barriers after LPS stimulation.

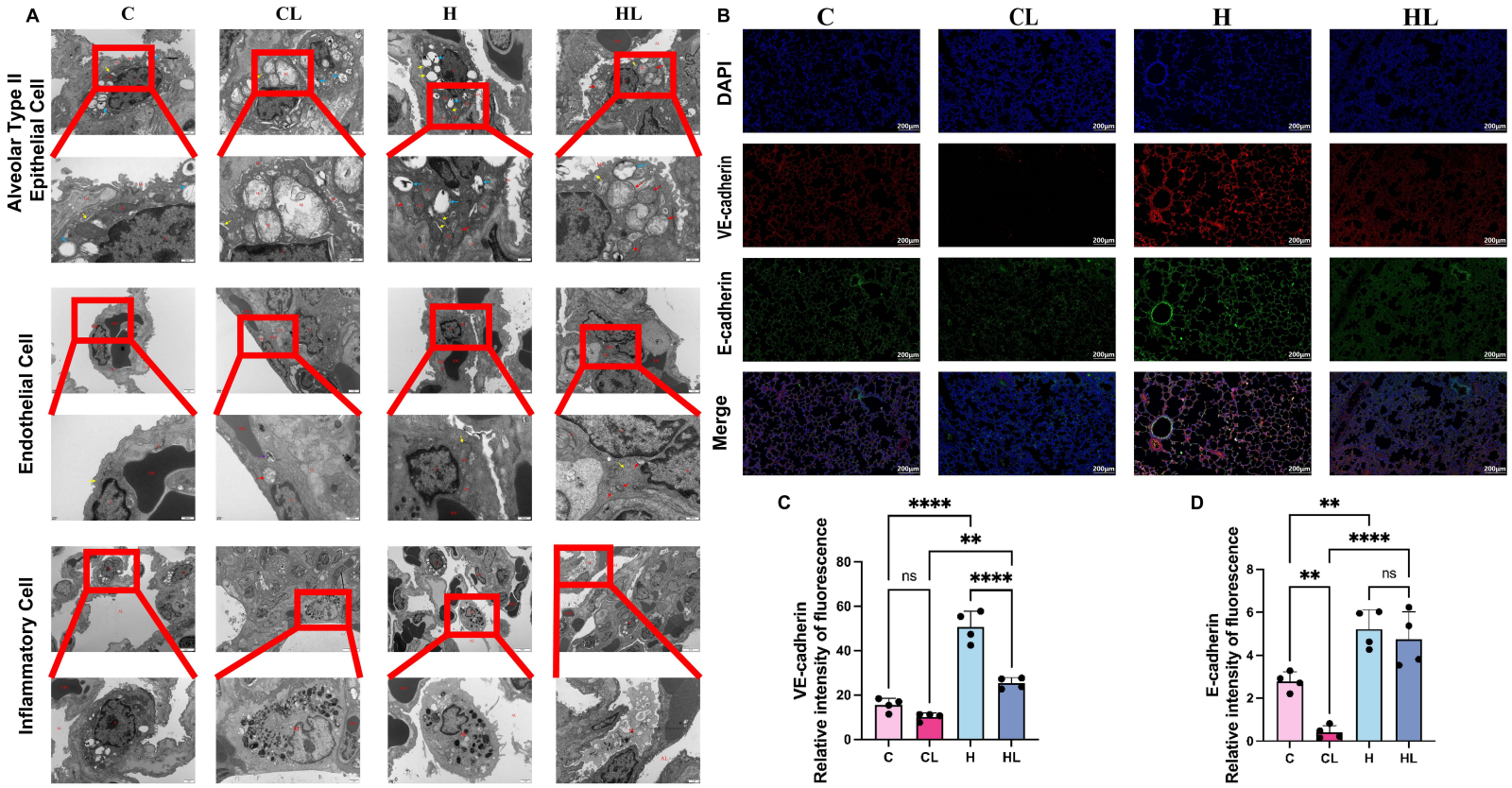

Figure 7 HAP attenuates injury to junctional structures of the pulmonary vascular and alveolar barriers.(**A**) HAP attenuated ultrastructural injury in lung tissue (n=3). From top to bottom: alveolar type II epithelial cells, vascular endothelial cells, and inflammatory cells. N, nucleus; Mi, mitochondria; RER, rough endoplasmic reticulum; TJ, junctional structure; Co, collagen fibers; Mv, microvilli; RBC, red blood cells; Ed, endothelial cell; AL, alveolar lumen; M, macrophage. ↑ in blue, lamellar bodies; ↑ in red, mitochondria;↑ in purple, lysosomes;↑ in yellow, rough endoplasmic reticulum. Scale bars: 1μm; 500nm. (**B**) Representative immunofluorescence images of lung tissue (scale bar=200μm), in which VE-cadherin is shown in red, E-cadherin in green, and DAPI-stained nuclei in blue. (**C**) Relative fluorescence intensity of VE-cadherin in each group analyzed using ImageJ software (n=4). (**D**) Relative fluorescence intensity of E-cadherin in each group analyzed using ImageJ software (n=4). ns, $P>0.05$; $^{**}P<0.01$; $^{****}P<0.0001$.

https://doi.org/10.2147/JIR.S577600

Discussion

HAP Attenuates Lung Tissue Injury Under Inflammatory Stimulation and Improves Related Functional Parameters

At the whole-organ level, this study confirmed that HAP exerts a certain attenuating effect on LPS-induced lung injury. Compared with the CL group, the HL group showed less severe gross pulmonary exudation and hemorrhage, a smaller decrease in the lung dry/wet weight ratio, reduced inflammatory cell infiltration on H&E staining, and better preservation of alveolar architecture, indicating that under the same inflammatory stimulus, lung tissue in HAP-treated rats is less likely to rapidly develop marked leakage and structural destruction. Consistent with the alleviation of histological injury, inflammation- and oxidative stress-related indicators in the HL group were overall lower than those in the CL group, suggesting that after HAP intervention, the degrees of inflammation and oxidative stress in lung tissue under acute inflammatory stimulation were lower. Previous studies have shown that reactive oxygen species may transiently increase during the early phase of high-altitude hypoxic exposure, whereas with the establishment of long-term adaptation, hypoxia-related signaling and antioxidant defense mechanisms are gradually developed, thereby buffering, to some extent, the oxidative stress burden imposed by sustained hypoxia.[27] Taken together with the present findings, the overall stress response may be milder when HAP-treated organisms are subjected to inflammatory stimulation.

Arterial blood gas analysis further suggested that this protective effect is reflected not only in milder histological injury, but also in changes in lung function. Compared with the CL group, the HL group showed overall better oxygenation-related parameters, whereas oxygenation declined more markedly in the CL group, indicating that after HAP treatment, lung tissue retained relatively better gas exchange capacity under inflammatory stimulation. It should be noted that increases in Hb, Hct, and CaO_2 are themselves fundamental physiological adaptations to high altitude and may indeed confer a certain advantage in oxygen transport to the HL group.[28,29] However, if the effect were attributable solely to increased oxygen-carrying capacity, it would be difficult to simultaneously explain the overall benefits observed in the HL group, including reduced pulmonary leakage, alleviated pathological injury, and better preservation of alveolar structure. Therefore, the present study suggests that the effect of HAP is not limited to improving oxygen delivery, but also includes attenuation of lung tissue injury under inflammatory stimulation. This finding is also consistent with our previous studies: in a retrospective study of patients undergoing cardiac surgery, HAP was associated with a lower incidence of major adverse cardiovascular events and less severe postoperative myocardial injury;[23] in our previous animal experiments, HAP-treated rats likewise showed milder lung injury after LPS stimulation, suggesting that HAP may exert a certain cross-organ protective effect.[25] Changes in metabolic parameters also support this conclusion. In the present study, the increase in lactate was smaller in the HL group, and its overall level was lower than that in the CL group. At the same time, blood glucose decreased markedly in the CL group, whereas no significant decrease was observed in the HL group, indicating that changes in blood glucose and lactate were more stable under inflammatory stimulation after HAP treatment. This is consistent with our previous perioperative clinical observations, in which patients adapted to high altitude exhibited more stable changes in blood glucose and lactate under stress conditions.[24] Taken together, HAP enables lung tissue to exhibit milder injury, less fluid leakage, better oxygenation status, and more stable metabolic changes after inflammatory stimulation, thereby providing an experimental basis for further analysis of its effects at the level of the alveolar-capillary barrier.

HAP Affects the Transcriptional Characteristics of Alveolar-Capillary Barrier-Related Cells

The above findings showed that HAP attenuated LPS-induced lung injury, reduced exudation, and improved oxygenation. To examine the cellular basis associated with this protective effect, the present study investigated transcriptional changes in alveolar-capillary barrier-related cells at the single-cell level, with a particular focus on endothelial cells on the vascular side of the barrier, epithelial cells on the alveolar side, and macrophages involved in barrier regulation.

Endothelial cells are the core structural component on the vascular side of the alveolar-capillary barrier, and their state directly determines changes in vascular permeability and the degree of fluid extravasation.[30] In the present study, genes upregulated in the CL group were mainly enriched in pathways related to endoplasmic reticulum stress and the unfolded

protein response, including Ddit3, Xbp1, Hsp90b1, and Hspb1,[31–34] suggesting that stress-related changes were more prominent under inflammatory stimulation in this group. In contrast, genes upregulated in the HL group were more enriched in categories related to focal adhesion and actin cytoskeletal remodeling, including Flnb, Actr3, Vcl, and Tes. Previous studies have shown that FLNB is involved in S1PR1 membrane surface localization,[35] that the Arp2/3 complex containing Actr3 can drive the formation of junction-associated membrane protrusions and promote renewal at VE-cadherin sites,[36] that Vcl enhances endothelial barrier integrity and reduces vascular leakage,[37] and that Tes is related to adhesive structures and the recognition of force-bearing actin.[38] These findings are consistent with the reduced exudation and milder barrier disruption observed in the HL group in the present study, and together suggest that, after HAP treatment, endothelial cells are more inclined toward expression patterns related to junction maintenance and structural stability.

Notably, a distinct endothelial cell subset with an activated transcriptional profile was observed in our analysis. For descriptive convenience only, this subset was provisionally referred to as activated endothelial cells (aiECs), characterized by high expression levels of Cx3cl1 and Fxyd5, as well as elevated expression of Il6, Ccl7, and Vcam1. Meanwhile, this subset also exhibited relatively high expression of Anxa1, Timp3, Cst3, Tm4sf1, and Mgp, implying that it may not represent a purely pro-inflammatory endothelial population. Pseudotime analysis showed that gCap cells bifurcated into two major branches leading to aCap and aiEC, respectively, and that more HL-group cells were distributed at the terminal end of the aiEC branch. S100a10 and Anxa2 gradually increased along this trajectory and reached their peaks at the aiEC-enriched end. Annexin A2, as a membrane phospholipid-binding protein, plays an important role in membrane localization and maintenance of adhesion junctions.[39] Previous studies have shown that Anxa2 deficiency leads to impaired pulmonary microvascular endothelial barrier function and is accompanied by abnormal phosphorylation of VE-cadherin.[40] S100a10 is an important binding partner of Anxa2, and the annexin A2/S100A10 heterotetramer formed by the two is closely related to membrane-cytoskeletal organization and cell-surface protein localization.[41] Taken together with the relative enrichment of HL-group cells in the aiEC branch and the peak expression of Anxa2/S100a10 in this branch, these findings suggest that Anxa2/S100a10-related membrane-cytoskeletal remodeling is consistent with the better preservation of endothelial junctions in the HL group. However, whether this process directly participates in HAP-related protection still requires further functional validation.

Compared with the endothelial side, the key role of the alveolar epithelial side is not to prevent fluid extravasation,[42] but rather to maintain the integrity of the alveolar interface, promote fluid clearance, and initiate timely repair after injury.[19] In the present study, the proportion of AT1 cells was increased in the HL group, whereas the proportion of Tuft cells was increased in the CL group. AT2 cells are an important regenerative source for alveolar repair and can transdifferentiate into AT1 cells to replenish the alveolar-capillary barrier,[43] while the state of AT1 cells is closely related to restoration of barrier continuity.[44] Therefore, the higher proportion of AT1 cells in the HL group may reflect earlier emergence of structural recovery-related changes in epithelial cells after inflammatory stimulation following HAP treatment. Conversely, the relative proportion of Tuft cells was elevated in the CL group. As documented in previous studies, Tuft cells constitute a rare epithelial subset endowed with chemosensory and immunomodulatory properties. These cells are capable of undergoing proliferation during inflammation- or injury-driven airway remodeling and can secrete proinflammatory mediators to amplify local immune responses.[45] Accordingly, the increased abundance of Tuft cells observed in the CL group herein is most likely indicative of exacerbated epithelial injury under inflammatory stress. Further comparison of differentially expressed genes between the two groups showed that the CL group mainly upregulated Sdf2l1, Ifi27, Cyba, and Nos2, indicating a greater tendency toward proteostatic stress, endoplasmic reticulum stress, and inflammatory responses; in contrast, genes upregulated in the HL group, including Npnt, Cldn18, Scnn1a, and Sparc, were more closely related to membrane structure, adhesion, and fluid clearance. Among these, Cldn18 is an important component of alveolar epithelial tight junctions and is closely associated with alveolar barrier permeability and homeostasis;[46] Scnn1a encodes the α-subunit of the epithelial sodium channel and is closely related to alveolar fluid clearance;[47] Npnt is associated with the basement membrane/cell adhesion network;[48,49] and Sparc is involved in extracellular matrix remodeling and regulation of the injury-repair microenvironment.[50] In addition, pseudotime analysis showed that more CL-group cells were located at the beginning of the trajectory, whereas HL-group cells were distributed across multiple stages of the trajectory; Atf3 and Btg2 gradually decreased with pseudotime,

whereas Col4a3 and Col4a4 gradually increased. These findings suggest that, compared with the CL group, epithelial cells in the HL group not only show less injury- and inflammation-related expression, but also exhibit more expression features related to membrane structure, adhesion, and fluid clearance.

In addition to structural cells, macrophages also influence whether lung barrier injury is further aggravated. In the present study, there was no significant difference in the overall proportions of macrophage subclusters, but their transcriptional changes were clearly different. Differential genes in the CL group were more enriched in pro-inflammatory, granulocyte recruitment, and interferon-related pathways, whereas those in the HL group were more enriched in pathways related to the extracellular region, extracellular space, and regulation of cell proliferation, indicating that the effect of HAP on macrophages was mainly reflected in distinct transcriptional responses after inflammatory stimulation. Increased expression of S100a9, Ptgs2, Aim2, and Ltb4r1 in the CL group suggested a greater tendency toward inflammation- and injury-related changes.[51–55] In contrast, the HL group upregulated genes such as Arg1, Anxa1, Thbd, and Timp1. Among these, Anxa1 can inhibit NF-κB activation and alleviate LPS-induced acute lung injury,[56] Thbd has protective effects in multiple lung injury models,[57–59] and Timp1 is related to extracellular matrix regulation in lung tissue.[60] Pseudotime analysis further showed that more HL-group cells were located at the beginning of the trajectory, mainly composed of mature tissue-resident alveolar macrophages, whereas the proportion of cells at the terminal end of the interferon-stimulation-related branch was higher in the CL group.

Overall, the single-cell results of the present study do not support a simple interpretation that HAP-related pulmonary protection can be attributed to a single cell type or a single molecular pathway. Rather, they suggest that this protection may be manifested as coordinated alterations in the stress-response patterns of multiple barrier-related cell types. Specifically, endothelial cells appear more biased toward programs related to junction and cytoskeletal maintenance, epithelial cells toward expression related to membrane structure and fluid clearance, and macrophages toward reduced inflammatory and interferon-like transcriptional features. Together, these changes provide a cellular-level explanation for the milder lung injury and better-preserved barrier integrity observed in the HL group.

Structural Evidence Supports That HAP Attenuates Disruption of the Alveolar-Capillary Barrier

In the preceding single-cell analysis, endothelial cells and epithelial cells in the HL group were found to be more biased toward programs related to junctional maintenance and repair. The TEM and junctional protein findings in the present study further indicate that these gene-expression differences are consistent with histological evidence of better preservation of alveolar-capillary barrier structure.

TEM findings in the present study showed that, compared with the CL group, ultrastructural injury in vascular endothelial cells and AT2 cells was milder in the HL group, intercellular junctions were better preserved, and mitochondrial swelling and structural disruption were also less severe. Because the integrity of endothelial and epithelial cells is the basis for maintaining low permeability of the alveolar-capillary barrier, this better-preserved ultrastructural appearance provides a reasonable explanation for the reduced exudation and improved oxygenation observed above. Immunofluorescence further showed that the fluorescence intensity and continuity of VE-cadherin and E-cadherin were both higher in the H group than in the C group, and that after LPS stimulation, the HL group still showed significantly better preservation than the CL group. VE-cadherin is a core molecule of endothelial adherens junctions, and its continuity and stability directly affect endothelial barrier integrity and vascular permeability. Previous studies have shown that promoting reconstruction of VE-cadherin junctions helps restore pulmonary fluid balance, improve lung structure, and facilitate resolution of lung injury.[61,62] E-cadherin is an important component of epithelial adherens junctions, and reduced expression, increased cleavage, or disrupted membrane localization usually indicates impaired continuity of the epithelial barrier and is involved in processes related to amplification of inflammation and impaired repair.[63,64] Taken together with the TEM observations, junctional protein findings, and the single-cell results described above, the present study suggests that, in this model, HAP is associated with better preservation of alveolar-capillary barrier structure, stronger junctional protein signals, and less leakage, and that better-preserved barrier integrity may be one of the important bases underlying its pulmonary protective effect.

This finding is in good agreement with our previous work. In our earlier clinical study,[24] patients adapted to high altitude showed a lower incidence of pleural effusion among postoperative pulmonary complications after hepatectomy. Although pleural effusion is influenced by multiple factors, a reduction in pleural fluid still essentially suggests less severe pulmonary fluid leakage. In addition, in our previous HAP-intervention study using an LPS-induced intestinal injury model, HAP attenuated intestinal tissue injury and exudation and preserved the relative integrity of tight junction proteins such as ZO-1 and Occludin, suggesting that the effects of HAP on barrier function may be shared across organs.[65] Although the intestinal barrier and the alveolar-capillary barrier are not identical in structure, both depend on the integrity of junctional structures to limit abnormal leakage. This is consistent with the findings of the present study, in which the HL group showed reduced exudation, better-preserved junctions, and improved oxygenation, and further strengthens the credibility of our conclusions.

When the TEM findings, junctional protein analysis, and the above results are considered together, HAP-related pulmonary protection appears to involve more than simple attenuation of inflammatory responses. More importantly, injury to the alveolar-capillary barrier is milder after inflammatory stimulation, leading to reduced fluid leakage and, consequently, less alveolar compression and less severe impairment of oxygenation. This is consistent with our previous clinical and animal findings and suggests that HAP may induce a pulmonary protective state characterized by endogenous barrier protection.

Despite these findings, the present study still has several limitations. First, an LPS-induced model was used, which mainly reflects features of lung injury caused by inflammatory stimulation; the role of HAP in other types of lung injury remains to be further investigated. Second, observations in the present study were mainly focused on the acute phase, and the subsequent repair process and long-term outcomes were not dynamically evaluated. Third, although the present study analyzed changes in key cell populations by integrating single-cell results with structural evidence and identified several candidate molecules, no in vitro cell experiments or functional intervention studies were performed. Therefore, no direct conclusions can yet be drawn regarding the upstream signals and molecular mechanisms underlying HAP-related protection. Accordingly, the current mechanistic interpretation remains largely at the level of association rather than causal proof. Future studies integrating different models, multi-time-point observations, and in vivo and in vitro functional intervention experiments are still needed to further clarify the specific mechanisms by which HAP attenuates alveolar-capillary barrier injury.

Conclusion

This study showed that HAP was associated with better preservation of the alveolar-capillary barrier, as evidenced by reduced pulmonary edema, improved oxygenation, stronger junctional protein signals, and better preserved barrier structure in HAP-treated rats under LPS challenge. This protective effect was accompanied by distinct transcriptional characteristics in endothelial cells, epithelial cells, and macrophages. These findings suggest that HAP-related pulmonary protection may be associated with coordinated alterations in the responses of barrier-related cells.

Data Sharing Statement

The datasets generated during and/or analysed during the current study are available from the corresponding author on reasonable request. The raw scRNA-sequence data reported in this paper have been deposited in the Genome Sequence Archive (Genomics, Proteomics & Bioinformatics 2025) in National Genomics Data Center (Nucleic Acids Res 2025), China National Center for Bioinformation / Beijing Institute of Genomics, Chinese Academy of Sciences (GSA: CRA041550) that are publicly accessible at https://ngdc.cncb.ac.cn/gsa/browse/CRA041550.

Ethics Approval

This work was approved by the Ethics Committee for Basic and Clinical Research of Sichuan Provincial People's Hospital (Date:2024.7.15;NO.2024-419).

Author Contributions

Ruixuan Wang: Investigation, Visualization, Data curation,Writing - original draft
Yu Zhang: Investigation, Validation, Writing - original draft
Wantian Zhang: Investigation, Formal analysis, Data curation,Writing - original draft

Mei Gong: Investigation, Writing - review and editing
Danyang Zhao: Investigation, Resources, Formal analysis, Writing - review & editing
Chunhua Chen: Investigation, Conceptualization,Writing - review and editing, Supervision
Wei Chen: Investigation, Data curation, Supervision, Validation, Writing - review & editing
Qian Lei: Conceptualization, Supervision, Project administration, Funding acquisition, Methodology, Writing - original draft, Writing - review & editing
Si Zeng: Conceptualization, Supervision, Project administration, Funding acquisition, Writing - original draft, Writing-review and editing, Methodology, Visualization

All authors took part in drafting, revising or critically reviewing the article; gave final approval of the version to be published; have agreed on the journal to which the article has been submitted; and agree to be accountable for all aspects of the work.

Funding

This work was supported by The National Natural Science Foundation of China (No. 82202071,82470290), Research Project on Innovative Application of Professional Competencies in Clinical Specialties by the National Health Commission Talent Exchange and Service Center (RCLX2315027),and Scientific research cooperation Project of North Sichuan Medical College (No.CBY25-ZXZDA06).

Disclosure

The authors have no relevant financial or non-financial interests to disclose.

References

1. Forrer A, Gaisl T, Sevik A, et al. Partial pressure of arterial oxygen in healthy adults at high altitudes: a systematic review and meta-analysis. *JAMA Network Open*. 2023;6(6):e2318036. doi:10.1001/jamanetworkopen.2023.18036
2. Lira-Mejia B, Calderon-Romero R, Ordaya-Fierro J, et al. Impact of exposure duration to high-altitude hypoxia on oxidative homeostasis in rat brain regions. *Int J Mol Sci*. 2025;26(17):178714. doi:10.3390/ijms26178714
3. Savina Y, Pichon AP, Lemaire L, et al. Micro- and macrovascular function in the highest city in the world: a cross sectional study. *Lancet Reg Health Am*. 2024;38:100887. doi:10.1016/j.lana.2024.100887
4. Ibrahim E, Sohail SK, Ihunwo A, Eid RA, Al-Shahrani Y, Rezigalla AA. Effect of high-altitude hypoxia on function and cytoarchitecture of rats' liver. *Sci Rep*. 2025;15(1):12771. doi:10.1038/s41598-025-97863-x
5. Carin R, Faucher C, Connes P, et al. Persisting elevation of total hemoglobin mass after altitude training in elite swimmers: a potential role of prolonged erythrocyte survival. *Am J Physiol Heart Circ Physiol*. 2025;329(4):H789–H800. doi:10.1152/ajpheart.00334.2025
6. Wu W, Chen G, Zhang X, et al. The effect of long-term exposure to moderate high altitude on adipokines and insulin sensitivity. *Cytokine*. 2025;185:156823. doi:10.1016/j.cyto.2024.156823
7. Yin J, Lv J, Yang S, et al. Multi-omics reveals immune response and metabolic profiles during high-altitude mountaineering. *Cell Rep*. 2025;44 (1):115134. doi:10.1016/j.celrep.2024.115134
8. Lan Q, Wang K, Meng Z, et al. Roxadustat promotes hypoxia-inducible factor-1α/vascular endothelial growth factor signalling to enhance random skin flap survival in rats. *Int Wound J*. 2023;20(9):3586–3598. doi:10.1111/iwj.14235
9. Lei F-J, Chiang J-Y, Chang H-J, et al. Cellular and exosomal GPx1 are essential for controlling hydrogen peroxide balance and alleviating oxidative stress in hypoxic glioblastoma. *Redox Biol*. 2023;65:102831. doi:10.1016/j.redox.2023.102831
10. Zazzeron L, Shimoda K, Lichtenegger P, et al. Prolonged postnatal hypoxia impairs lung development and causes severe pulmonary hypertension in mice. *J Am Heart Assoc*. 2025;14(20):e042608. doi:10.1161/JAHA.125.042608
11. Yang P, Sjoding MW. Acute respiratory distress syndrome: definition, diagnosis, and routine management. *Crit Care Clin*. 2024;40(2):309–327. doi:10.1016/j.ccc.2023.12.003
12. Shi Y, Wang L, Yu S, Ma X, Li X. Risk factors for acute respiratory distress syndrome in sepsis patients: a retrospective study from a tertiary hospital in China. *BMC Pulm Med*. 2022;22(1):238. doi:10.1186/s12890-022-02015-w
13. Herbst CJ, Lopez-Rodriguez E, Gluhovic V, et al. Characterization of commercially available human primary alveolar epithelial cells. *Am J Respir Cell Mol Biol*. 2024;70(5):339–350. doi:10.1165/rcmb.2023-0320MA
14. Atmowihardjo LN, Heijnen NFL, Smit MR, et al. Biomarkers of alveolar epithelial injury and endothelial dysfunction are associated with scores of pulmonary edema in invasively ventilated patients. *Am J Physiol Lung Cell Mol Physiol*. 2023;324(1):L38–L47. doi:10.1152/ajplung.00185.2022
15. Brune K, Frank J, Schwingshackl A, Finigan J, Sidhaye VK. Pulmonary epithelial barrier function: some new players and mechanisms. *Am J Physiol Lung Cell Mol Physiol*. 2015;308(8):L731–L745. doi:10.1152/ajplung.00309.2014
16. Su Y, Lucas R, Fulton DJR, Verin AD. Mechanisms of pulmonary endothelial barrier dysfunction in acute lung injury and acute respiratory distress syndrome. *Chin Med J Pulm Crit Care Med*. 2024;2(2):80–87. doi:10.1016/j.pccm.2024.04.002
17. Millar MW, Najar RA, Slavin SA, et al. MTOR maintains endothelial cell integrity to limit lung vascular injury. *J Biol Chem*. 2024;300 (12):107952. doi:10.1016/j.jbc.2024.107952

18. Huang T, Chen D, Ye W, et al. Effect and mechanism of apelin on lipopolysaccharide induced acute pulmonary vascular endothelial barrier dysfunction. *Sci Rep*. 2023;13(1):1560. doi:10.1038/s41598-023-27889-6
19. Shi QQ, Huang YH, Li YF, et al. PEBP4 deficiency aggravates LPS-induced acute lung injury and alveolar fluid clearance impairment via modulating PI3K/AKT signaling pathway. *Cell Mol Life Sci*. 2024;81(1):133. doi:10.1007/s00018-024-05168-5
20. Wang Y, Wang L, Ma S, Cheng L, Yu G. Repair and regeneration of the alveolar epithelium in lung injury. *FASEB J*. 2024;38(8):e23612. doi:10.1096/fj.202400088R
21. Guttenberg MA, Vose AT, Birukova A, et al. Tissue-Resident alveolar macrophages reduce ozone-induced inflammation via MerTK-mediated efferocytosis. *Am J Respir Cell Mol Biol*. 2024;70(6):493–506. doi:10.1165/rcmb.2023-0390OC
22. Feng N, Li Y, Guo F, et al. Fibroblast growth factor 10 alleviates LPS-induced acute lung injury by promoting recruited macrophage M2 polarization. *Inflammation*. 2025;48(4):1828–1838. doi:10.1007/s10753-024-02158-4
23. Lei L, Liu M, Ma D, et al. Cardioprotective effects of high-altitude adaptation in cardiac surgical patients: a retrospective cohort study with propensity score matching. *Front Cardiovasc Med*. 2024;11:1347552. doi:10.3389/fcvm.2024.1347552
24. Luo Q, Zhang Y, Gu S, Liu L, Zeng S, Lei Q. High-altitude adaptation as a protective factor against postoperative pulmonary complications in liver resection: a prospective matched cohort study. *BMC Anesthesiol*. 2025;25(1):352. doi:10.1186/s12871-025-03215-7
25. Zhang W, Wang R, Zhang Y, Lei Q, Zeng S. Lactate regulation in high-altitude hypoxic adaptation attenuates LPS-Induced acute lung injury: links to glucose metabolism and anti-inflammatory therapeutic potential. *Crit Care*. 2026;30(1):59. doi:10.1186/s13054-026-05905-1
26. Du Sert N P, Hurst V, Ahluwalia A, et al. The ARRIVE guidelines 2.0: Updated guidelines for reporting animal research. *Br J Pharmacol*. 2020;177(16):3617–3624. doi:10.1111/bph.15193
27. Lin HJ, Wang CT, Niu KC, et al. Hypobaric hypoxia preconditioning attenuates acute lung injury during high-altitude exposure in rats via up-regulating heat-shock protein 70. *Clin Sci*. 2011;121(5):223–231. doi:10.1042/CS20100596
28. Ye S, Sun J, Craig SR, et al. Higher oxygen content and transport characterize high-altitude ethnic Tibetan women with the highest lifetime reproductive success. *Proc Natl Acad Sci U S A*. 2024;121(45):e2403309121. doi:10.1073/pnas.2403309121
29. Mancera-Soto EM, Chamorro-Acosta ML, Ramos-Caballero DM, Torrella JR, Cristancho-Mejia E. Effect of hypobaric hypoxia on hematological parameters related to oxygen transport, blood volume and oxygen consumption in adolescent endurance-training athletes. *J Exerc Sci Fit*. 2022;20(4):391–399. doi:10.1016/j.jesf.2022.10.003
30. Zhang J, Cao Y, Shu W, Dong S, Sun Y, Ma X. Neutrophil-derived heparin-binding protein increases endothelial permeability in acute lung injury by promoting TRIM21 and the ubiquitination of P65. *Cell Biol Toxicol*. 2025;41(1):55. doi:10.1007/s10565-025-10005-x
31. Zhuang H, Hudson E, Han S, et al. Microvascular lung injury and endoplasmic reticulum stress in systemic lupus erythematosus-associated alveolar hemorrhage and pulmonary vasculitis. *Am J Physiol Lung Cell Mol Physiol*. 2022;323(6):L715–L729. doi:10.1152/ajplung.00051.2022
32. Marzec M, Eletto D, Argon Y. GRP94: An HSP90-like protein specialized for protein folding and quality control in the endoplasmic reticulum. *Biochim Biophys Acta*. 2012;1823(3):774–787. doi:10.1016/j.bbamcr.2011.10.013
33. Wang S, Hu L, Fu Y, et al. Inhibition of IRE1alpha/XBP1 axis alleviates LPS-induced acute lung injury by suppressing TXNIP/NLRP3 inflammasome activation and ERK/p65 signaling pathway. *Respir Res*. 2024;25(1):417. doi:10.1186/s12931-024-03044-1
34. Sun M, Yang Q, Tan Y, et al. The transcription factor DDIT3 regulates macrophage function by inhibiting KLF10 to attenuate ALI/ARDS inflammation. *Inflammation*. 2026;49(1):65. doi:10.1007/s10753-026-02451-4
35. Zhao X, Kiyozuka K, Konishi A, Kawabata-Iwakawa R, Minamishima YA, Obinata H. Actin-binding protein filamin B regulates the cell-surface retention of endothelial sphingosine 1-phosphate receptor 1. *J Biol Chem*. 2023;299(7):104851. doi:10.1016/j.jbc.2023.104851
36. Abu Taha A, Taha M, Seebach J, Schnittler HJ. ARP2/3-mediated junction-associated lamellipodia control VE-cadherin-based cell junction dynamics and maintain monolayer integrity. *Mol Biol Cell*. 2014;25(2):245–256. doi:10.1091/mbc.E13-07-0404
37. Van der Stoel MM, Kotini MP, Schoon RM, Affolter M, Belting HG, Huveneers S. Vinculin strengthens the endothelial barrier during vascular development. *Vasc Biol*. 2023;5(1):VB–22–0012. doi:10.1530/VB-22-0012
38. Sala S, Oakes PW. Stress fiber strain recognition by the LIM protein testin is cryptic and mediated by RhoA. *Mol Biol Cell*. 2021;32(18):1758–1771. doi:10.1091/mbc.E21-03-0156
39. Sveeggen TM, Abbey CA, Smith RL, Salinas ML, Chapkin RS, Bayless KJ. Annexin A2 modulates phospholipid membrane composition upstream of Arp2 to control angiogenic sprout initiation. *FASEB J*. 2023;37(1):e22715. doi:10.1096/fj.202201088R
40. Luo M, Flood EC, Almeida D, et al. Annexin A2 supports pulmonary microvascular integrity by linking vascular endothelial cadherin and protein tyrosine phosphatases. *J Exp Med*. 2017;214(9):2535–2545. doi:10.1084/jem.20160652
41. Abd El-Aleem SA, Dekker LV. Assessment of the cellular localisation of the annexin A2/S100A10 complex in human placenta. *J Mol Histol*. 2018;49(5):531–543. doi:10.1007/s10735-018-9791-2
42. Shao S, Zhang N, Specht GP, et al. Pharmacological expansion of type 2 alveolar epithelial cells promotes regenerative lower airway repair. *Proc Natl Acad Sci U S A*. 2024;121(16):e2400077121. doi:10.1073/pnas.2400077121
43. Sucre JM, Bock F, Negretti NM, et al. Alveolar repair following LPS-induced injury requires cell-ECM interactions. *JCI Insight*. 2023;8(14):e167211. doi:10.1172/jci.insight.167211
44. Guild J, Juul NH, Andalon A, et al. Evidence for lung barrier regeneration by differentiation prior to binucleated and stem cell division. *J Cell Biol*. 2023;222(12):e202212088. doi:10.1083/jcb.202212088
45. Barr J, Gentile ME, Lee S, et al. Injury-induced pulmonary tuft cells are heterogenous, arise independent of key Type 2 cytokines, and are dispensable for dysplastic repair. *Elife*. 2022;11:e78074. doi:10.7554/eLife.78074
46. Li G, Flodby P, Luo J, et al. Knockout mice reveal key roles for claudin 18 in alveolar barrier properties and fluid homeostasis. *Am J Respir Cell Mol Biol*. 2014;51(2):210–222. doi:10.1165/rcmb.2013-0353OC
47. Gao Y, Cao F, Tian X, et al. Inhibition the ubiquitination of ENaC and Na,K-ATPase with erythropoietin promotes alveolar fluid clearance in sepsis-induced acute respiratory distress syndrome. *Biomed Pharmacother*. 2024;174:116447. doi:10.1016/j.biopha.2024.116447
48. Wilson CL, Hung CF, Burkel BM, Ponik SM, Gharib SA, Schnapp LM. Nephronectin is required to maintain right lung lobar separation during embryonic development. *Am J Physiol Lung Cell Mol Physiol*. 2023;324(3):L335–L344. doi:10.1152/ajplung.00505.2021
49. Guo J, Wang Y, Liu Q, et al. Nephronectin (NPNT) is a crucial determinant of idiopathic pulmonary fibrosis: modulating cellular senescence via the ITGA3/YAP1 signaling axis. *Adv Sci*. 2025;12(32):e01956. doi:10.1002/advs.202501956

50. Conforti F, Ridley R, Brereton C, et al. Paracrine SPARC signaling dysregulates alveolar epithelial barrier integrity and function in lung fibrosis. *Cell Death Discov*. 2020;6:54. doi:10.1038/s41420-020-0289-9
51. Gong C, Ma J, Deng Y, et al. S100A9(-/-) alleviates LPS-induced acute lung injury by regulating M1 macrophage polarization and inhibiting pyroptosis via the TLR4/MyD88/NFkappaB signaling axis. *Biomed Pharmacother*. 2024;172:116233. doi:10.1016/j.biopha.2024.116233
52. Nelin LD, Jin Y, Chen B, Liu Y, Rogers LK, Reese J. Cyclooxygenase-2 deficiency attenuates lipopolysaccharide-induced inflammation, apoptosis, and acute lung injury in adult mice. *Am J Physiol Regul Integr Comp Physiol*. 2022;322(2):R126–R135. doi:10.1152/ajpregu.00140.2021
53. Almatroudi A, Alsahli MA, Syed MA, Khan AA, Rahmani AH. Prostaglandin D2 attenuates lipopolysaccharide-induced acute lung injury through the modulation of inflammation and macrophage polarization. *Appl Sci*. 2022;12(12):6076.
54. Zhang H, Luo J, Alcorn JF, et al. AIM2 inflammasome is critical for influenza-induced lung injury and mortality. *J Immunol*. 2017;198 (11):4383–4393. doi:10.4049/jimmunol.1600714
55. Wang C, Zhang W, Guo Y, et al. GPR43 alleviates LPS-induced acute lung injury by inhibiting NLRP3 inflammasome activation via beta-arrestin 2. *Biol Direct*. 2026;21(1):16. doi:10.1186/s13062-025-00725-9
56. Huang H, Shi Y, Zhou Y. The protective effects of annexin A1 in acute lung injury mediated by Nrf2. *Immun Inflamm Dis*. 2025;13(1):e70111. doi:10.1002/iid3.70111
57. Kikuchi K, Kazuma S, Yamakage M. Recombinant thrombomodulin and recombinant antithrombin attenuate pulmonary endothelial glycocalyx degradation and neutrophil extracellular trap formation in ventilator-induced lung injury in the context of endotoxemia. *Respir Res*. 2024;25(1):330. doi:10.1186/s12931-024-02958-0
58. Hayase N, Doi K, Hiruma T, et al. Recombinant thrombomodulin prevents acute lung injury induced by renal ischemia-reperfusion injury. *Sci Rep*. 2020;10(1):289. doi:10.1038/s41598-019-57205-0
59. Iwashita Y, Zhang E, Maruyama J, et al. Thrombomodulin protects against lung damage created by high level of oxygen with large tidal volume mechanical ventilation in rats. *J Intensive Care*. 2014;2(1):57. doi:10.1186/s40560-014-0057-0
60. Dutta S, Zhu Y, Almuntashiri S, et al. PDGFRalpha-positive cell-derived TIMP-1 modulates adaptive immune responses to influenza A viral infection. *Am J Physiol Lung Cell Mol Physiol*. 2025;328(1):L60–L74. doi:10.1152/ajplung.00104.2024
61. Herwig MC, Tsokos M, Hermanns MI, Kirkpatrick CJ, Muller AM. Vascular endothelial cadherin expression in lung specimens of patients with sepsis-induced acute respiratory distress syndrome and endothelial cell cultures. *Pathobiology*. 2013;80(5):245–251. doi:10.1159/000347062
62. Xiong S, Hong Z, Huang LS, et al. IL-1beta suppression of VE-cadherin transcription underlies sepsis-induced inflammatory lung injury. *J Clin Invest*. 2020;130(7):3684–3698. doi:10.1172/JCI136908
63. Boxio R, Wartelle J, Nawrocki-Raby B, et al. Neutrophil elastase cleaves epithelial cadherin in acutely injured lung epithelium. *Respir Res*. 2016;17 (1):129. doi:10.1186/s12931-016-0449-x
64. Chen Z, Tang H, Gan S, et al. Ferroptosis mediates airway epithelial E-cadherin dysfunction in LPS-induced acute lung injury. *Pulm Pharmacol Ther*. 2024;84:102284. doi:10.1016/j.pupt.2023.102284
65. Wang R, Wen C, Lei Q, Zeng S. Lactate regulation may be a key factor in the protection of the intestinal barrier in sepsis under high-altitude hypoxic and hypobaric conditions. *Crit Care*. 2025;29(1):520. doi:10.1186/s13054-025-05793-x